Supporting Information for Multiple and Nonlocal Cation Redox in Ca-Ce-Ti-Mn Oxide Perovskites for Solar Thermochemical Applications

Robert B. Wexler[1], Gopalakrishnan Sai Gautam[1,2], Robert Bell[3], Sarah Shulda[3], Nicholas A. Strange[4], Jamie A. Trindell[5], Joshua D. Sugar[5], Eli Nygren[3,6], Sami Sainio[4], Anthony H. McDaniel[5], David Ginley[3], Emily A. Carter[1]*, and Ellen B. Stechel[7]*

[1]Department of Mechanical and Aerospace Engineering and the Andlinger Center for Energy and the Environment, Princeton University, Princeton, NJ 08544-5263, United States
[2]Department of Materials Engineering, Indian Institute of Science, Bengaluru, Karnataka 560012, India
[3]National Renewable Energy Laboratory, Golden, CO 80401 United States
[4]SLAC National Accelerator Laboratory, Menlo Park, CA 94025 United States
[5]Sandia National Laboratories, Livermore, CA 94550, United States
[6]University of California Santa Cruz, Santa Cruz, CA 95064 United States
[7]ASU LightWorks® and the School of Molecular Sciences, Arizona State University, Tempe, Arizona 85287-8204, United States
**Email: eac@princeton.edu, ellen.stechel@asu.edu*

Table of Contents

S1. Additional Computational Details

We calculated neutral oxygen vacancy formation energies using spin-polarized density functional theory (DFT) as implemented in the Vienna Ab initio Simulation Package (VASP) version 5.4.4.[1,2] We performed DFT calculations within the SCAN[3]+*U*[4–7] framework, where *U* were fit to relevant oxidation energies for Ce, Ti, V, Cr, Mn, Fe, Co, and Ni oxides.[8,9] This framework provides superior predictions of bulk thermodynamics, band gaps, and magnetic configurations in comparison to PBE, PBE+*U*, and SCAN.[8,9] We utilized all-electron, frozen-core, projector augmented-wave (PAW) potentials[10,11] to describe the ion-electron interactions, including the non-spherical contributions related to the electron density gradient and the kinetic energy density within the PAW spheres for the XC evaluation. We used the Accurate "precision" mode in VASP to avoid aliasing errors when setting fast-Fourier-transform and support grids. We employed an additional support grid for the more accurate estimation of augmentation charges and evaluated the projection operators in real space using VASP's fully automatic optimization scheme. We expanded the electronic wave function in a plane-wave basis with a kinetic-energy cutoff of 520 eV[8,9] and sampled only the Γ-point of the Brillouin zone due to the large size of the supercell (360 atoms). We applied a Gaussian smearing function with a width of 0.05 eV to improve self-consistent-field convergence. We performed collinear, spin-polarized calculations and initialized the atomic magnetic moments for the bulk in a ferromagnetic configuration with values of 0.6 μ_B for nominally nonmagnetic species (Ca^{2+}, Ce^{4+}, Ti^{4+}, and O^{2-}) and 4 μ_B for Mn^{3+}, which corresponds to its high spin state in an octahedral crystal field. For the vacancies, we initialized the atomic magnetic moments with bulk-optimized values.

S2. Stability

To compute the stability of $Ca_{2/3}Ce_{1/3}Ti_{1/3}Mn_{2/3}O_3$ (CCTM2112), we calculate its energy above the convex hull (E_{hull}), which is its energy of decomposition into the set of most stable materials at its chemical composition. To calculate E_{hull}, we use the phase diagram code in pymatgen[12–14] and SCAN+*U* total energies (E_{tot}) of materials containing Ca, Ce, Ti, Mn, and O from our prior work.[8,9,15] This code takes as input the E_{tot}s and compositions of these materials and returns the list of stable compositional coordinates in the phase diagram, where a stable compositional coordinate is a set of compounds in equilibrium – that define the chemical potentials of Ca, Ce, Ti, Mn, and O – that are on the convex hull. Our results show that CCTM2112 is metastable at 0 K, with an E_{hull} of 33 meV/atom, i.e., a ΔE for its decomposition reaction of

$$Ca_{2/3}Ce_{1/3}Ti_{1/3}Mn_{2/3}O_3 \rightarrow \frac{1}{9}Mn_2O_3 + \frac{2}{9}CaMn_2O_4 + \frac{1}{9}Ca_4Ti_3O_{10} + \frac{1}{3}CeO_2 \quad \text{(S1)}$$

where the products are the solid phases stable at Ca, Ce, Ti, Mn, and O mole fractions of 2/15, 1/15, 1/15, 2/15, and 9/15, respectively, at 0 K. 33 meV/atom is approximately equal to thermal energy at 298.15 K (i.e., k_BT = 26 meV/atom).

S3. Additional Synthesis Details

S3.1. Synthesis and Diffraction of (Ca,Ce)MnO_3

Attempts at synthesizing a ternary oxide in the phase space of (Ca,Ce)MnO_3 (CCM) were carried out and resulted in no formation of a perovskite phase bearing substantial stoichiometry of all three cations. Samples of CCM were prepared with cation molar ratios of 33.3% Ca, 16.7% Ce, and 50% Mn. Repeated 1773-K oxidation anneals and grinding steps failed to achieve formation of a single-phase or substantial ternary oxide component. In-operando X-ray diffraction (XRD) studies at SLAC BL 2-1 showed evidence of fractional substitution of Ce into a $CaMnO_3$ perovskite structure (with the preponderance of Ce remaining in CeO_2) under oxidizing conditions, but reduction at pO_2 of ≈1×10^{-4} bar at ≈973 K resulted in rapid (≈two-hour) dissolution of Ce almost entirely into the CeO_2 phase.

S3.2. Synthesis and Processing of (Ca,Ce)(Ti,Mn)O_3

(Ca,Ce)(Ti,Mn)O_3 (CCTM) with a bulk stoichiometry of $Ca_{0.65}Ce_{0.35}Ti_{0.3}Mn_{0.7}O_{3-\delta}$ was synthesized by mixing molar percentages of precursor powders: 32.5% CaO, 17.5% $Ce_2(CO_3)_3$, 17.5% MnO_2, 17.5% Mn_2O_3, and 15% TiO_2. Both Mn^{4+} and Mn^{3+} precursors are used to enable the Ce^{3+} precursor to reactively oxidize to Ce^{4+} while reducing Mn to predominately Mn^{3+} in the solid state. Samples were mixed in mortar and pestle, and then pressed in a one-inch steel die at 17,000 lbs. The pellet then was annealed at 1773 K for 20 hours in air. The resultant pellet was microporous due to escaping CO_2 from cerium precursor decomposition. The pellet then was re-ground in a mortar and pestle, re-pressed at 17,000 lbs. in a one-inch die, and then re-annealed at 1773 K for 20 hours in air. The pellet was dense after the second anneal. The pellet then was re-ground, pressed, and annealed under identical conditions. After this third anneal, the synthesis was considered complete. The pellet then was ground into a powder for X-ray absorption spectroscopy (XAS), XRD, and flow reactor testing.

Redox cycling was performed at 1473 K and cycled between air (pO_2 ≈ 0.2 atm) and house nitrogen (pO_2 ≈ 1×10^{-5} bar) in 16-hour increments. Aliquots of sample were extracted after each reduction and re-oxidation step. Changes in sample mass for each step are used to confirm reduction/re-oxidation Δδ.

S4. Special Quasirandom Structures

S4.1. Constructing a Special Quasirandom Structure for a 2D Random Alloy

To calculate the neutral oxygen vacancy formation energies of *Pnma* CCTM2112, we construct a special quasirandom structure (SQS)[16] using the icet code.[17] To explain SQS construction, consider a 2D model of a random alloy. In such a model, there are two types of atoms in the 2D system, green (with species variable $s = 1$) and blue (with species variable $s = -1$). For simplicity, let us assume that the fractions of green and blue atoms are both 1/2. We can define a cluster vector Γ, whose rank is determined by the number of unique interaction types within some threshold (number of interactions and distance between interacting atoms). Let us say that we only consider pair interactions $\leq r_{3NN}$, where r_{3NN} is the distance between a central atom and its third-nearest neighbors (NNs). In this case, the rank of the vector is three, and the three elements are the average correlations γ for first, second, and third NNs

$$\Gamma = \left[\gamma(r_{1NN}) \quad \gamma(r_{2NN}) \quad \gamma(r_{3NN})\right] \tag{S2}$$

For example, let us calculate the first element of the cluster vector. This is defined as the average interaction (i.e., the product of species variables) between the central atom ($i = 1$) and its first NNs ($j = 1 - 6$, orange circle in **Figure S1**)

$$\gamma(r_{1NN}) = \frac{1}{n_{sites}} \frac{1}{n_{1NN}} \sum_{i=1}^{n_{sites}} \sum_{j=1}^{n_{1NN}} s_i \cdot s_j \tag{S3}$$

First, we divide by the number of sites in the crystal (n_{sites}, because each site can have these first NN pair interactions) and the number of neighbors per site (n_{1NN}, in this case, it is six). We can split this sum into the term for the first central atom ($i = 1$) and other possible central atoms ($i > 1$).

$$\gamma(r_{1NN}) = \frac{1}{n_{sites}} \frac{1}{6} \left[\sum_{j=1}^{6} s_1 \cdot s_j + \sum_{i=2}^{n_{sites}} \sum_{k=1}^{6} s_i \cdot s_k \right] \tag{S4}$$

If we write out the sum for the first site $(1 \cdot 1 + 1 \cdot -1 + \ldots)$, then it is clear to see that the average interaction parameter is zero. Also, if we have a perfectly random distribution of blue and green atoms, we can expect that each of these terms for $i = 1$ and $i > 1$ should be close to zero. Therefore, the first element of Γ should be zero. Heterogeneous distributions (or clusters) of green and blue can lead to non-zero values of this first element. We then repeat this for all unique cluster types (pairs, triplets, different atom-atom distances for these pairs and triplets corresponding to specific distances between lattice sites, e.g., NNN lattice sites for r_{2NN}) to calculate all the relevant elements of Γ and compare this against what the perfectly random alloy would give. Each specified type (e.g., pair, triplet) and atom-atom distance gives rise to an entry in the cluster vector.

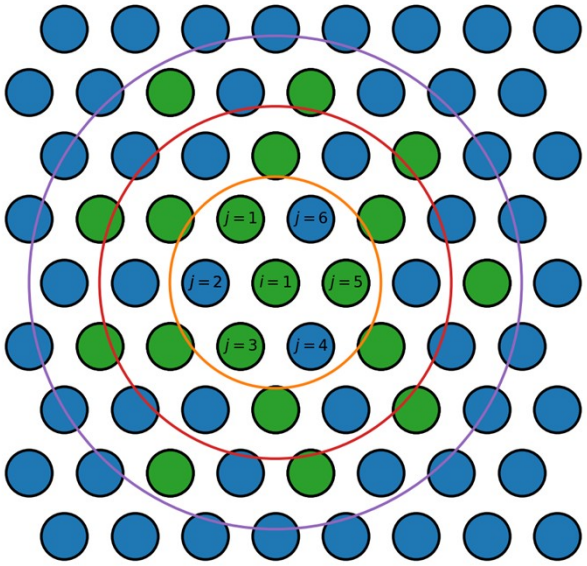

Figure S1. 2D model of a random alloy with green and blue atoms. Orange, red, and purple circles surround the first, second, and third nearest neighbor (NN) shells of the central atom with index $i = 1$. Atoms with indices $j = 1 - 6$ are the first NNs of atom $i = 1$.

S4.2 Optimizing a Special Quasirandom Structure for CCTM2112

SQS optimization involves the minimization of the following cost function

$$Q = -\omega L + \sum_{\alpha} \left| \Gamma_{\alpha} - \Gamma_{\alpha}^{target} \right| \tag{S5}$$

Here ω is the atom-atom distance (in Å) of the largest pair cluster with non-zero cluster vector deviation from the target (i.e., ideal solution) cluster vector Γ^{target} and L is a Lagrange multiplier defining the cost of cluster vector deviations from Γ^{target}.

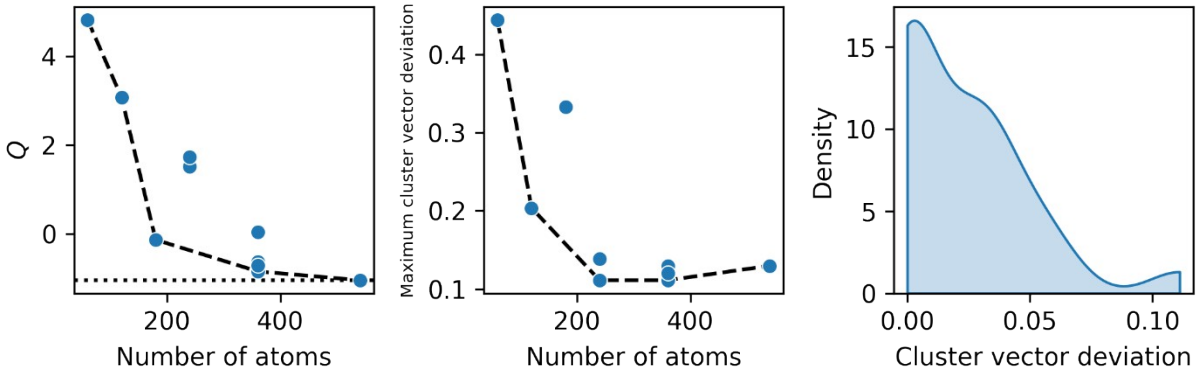

Figure S2. SQS construction for *Pnma* CCTM2112. The left and middle panels show the convergence of Q and the maximum cluster vector deviation ($|\Gamma - \Gamma^{target}|$) with respect to the number of atoms in the supercell, where the dashed lines indicate the convex hull. Some supercells have more than one data point [e.g., see the left panel] because we ran them in triplicate, each with a different random seed. The right panel shows the distribution of cluster

vector deviations for the 360-atom supercell with the smallest *Q* in the left panel. **Figure 1a** in the main text shows the crystal structure of the SQS. We used maximum distances of 7 and 4 Å to define/enumerate atom pairs and triplets, respectively.

Figure S2 presents the construction of the SQS for *Pnma* CCTM2112. The left panel shows that Q converges for 360-atom supercells. On the other hand, the middle panel indicates that the maximum cluster vector deviation is lowest for 240-atom supercells. For 360-atom supercells, the right panel shows an acceptable distribution of cluster vector deviations, which peaks near $|\Gamma - \Gamma^{target}| = 0$ and decays to zero above $|\Gamma - \Gamma^{target}| \lesssim 0.11$. We used the SQS shown in **Figure 1a** of the main text.

S5. H_2 Produced by State-of-the-Art Redox-Active Metal Oxides

For $BaCe_{0.25}Mn_{0.75}O_3$ (BCM), $Sr_{0.6}La_{0.4}Mn_{0.6}Al_{0.4}O_3$ (SLMA4664), and CeO_2, the absolute amount of H_2 produced has been reported in µmol H_2 per g oxide. To provide a more apples-to-apples comparison of H_2 production between different redox-active metal oxides that does not bias in favor of lighter compositions, we convert the 140 µmol H_2/g BCM, 194 µmol H_2/g SLMA4664, and 50 µmol H_2/g CeO_2 in **Figure 5** of **Reference 18** from µmol H_2/g oxide to mmol H_2/mol atom metal oxide. Note that the very last conversion divides the mmol/mol quantity by the number of atoms per formula unit of the metal oxide (five for perovskite ABO_3 and three for CeO_2).

$$\frac{140\ \mu mol\ H_2}{1\ g\ BCM} \times \frac{1\ mmol}{1000\ \mu mol} \times \frac{261.56\ g\ BCM}{1\ mol\ BCM} = \frac{36.6\ mmol\ H_2}{1\ mol\ BCM} \rightarrow \frac{7.3\ mmol\ H_2}{1\ mol\ atom\ BCM}$$

$$\frac{0.194\ mmol\ H_2}{1\ g\ SLMA4664} \times \frac{210.14\ g\ SLMA4664}{1\ mol\ SLMA4664} = \frac{40.8\ mmol\ H_2}{1\ mol\ SLMA4664} \rightarrow \frac{8.2\ mmol\ H_2}{1\ mol\ atom\ SLMA4664}$$

$$\frac{0.050\ mmol\ H_2}{1\ g\ CeO_2} \times \frac{172.11\ g\ CeO_2}{1\ mol\ CeO_2} = \frac{8.6\ mmol\ H_2}{1\ mol\ CeO_2} \rightarrow \frac{2.9\ mmol\ H_2}{1\ mol\ atom\ CeO_2}$$

In **Figure 4** of the main text, we report that CCTM2112 produces 10.4 mmol H_2/mol atom. To show how mmol H_2/mol atom oxide is a fairer metric than µmol H_2/g oxide, we convert the value for CCTM2112 from the former to the latter.

$$\frac{10.4 \times 10^3\ \mu mol\ H_2}{mol\ atom\ CCTM2112} \times 5\ atoms \times \frac{1\ mol\ CCTM2112}{174.00\ g\ CCTM2112} = \frac{298.8\ \mu mol\ H_2}{1\ g\ CCTM2112}$$

S6. Additional Empirical X-ray Diffraction Refinement Details

S6.1 Rietveld Refined Structure Information

The data used for Rietveld refinement for the as-synthesized $Ca_{0.65}Ce_{0.35}Ti_{0.3}Mn_{0.7}O_{3-\delta}$ sample was taken during XRD experiments at SSRL beamline 2-1. Rietveld refinements were performed using TOPAS-Academic, version 7.[19] Details on the XRD experiment and Rietveld refinement are given in **Table S1**. Additional information on the refinements results for CCTM's site mixing and isotropic displacement parameters are shown in **Table S2**, with CCTM geometric parameters given in **Table S3**. The CeO_2 impurity phase was simultaneously refined, with results in strong agreement with reported CeO_2 parameters. Refinement results for CeO_2 isotropic

displacement parameters (**Table S4**) and geometric parameters (**Table S5**) are reported. The .cif file for the CCTM structure, containing structure factors and other information, are available as an additional file.

Table S1. Experimental XRD and Rietveld refinement details

	CCTM	**Ceria**
Crystal data		
Chemical formula	$Ca_{0.65}Ce_{0.35}Ti_{0.3}Mn_{0.7}O_3$	CeO_2
M_r (g/mol)	175.91	172.12
Crystal system, space group	Orthorhombic, *Pnma*	Cubic, $Fm\bar{3}m$
Temperature (K)	300	300
a, *b*, *c* (Å)	5.61442 (13), 7.55658 (18), 5.35511 (13)	5.41109 (13), 5.41109 (13), 5.41109 (13)
α, β, γ (°)	90, 90, 90	90, 90, 90
Weight Percent (%)	98.76	1.24
V (Å^3)	227.20 (1)	158.44 (1)
Z	4	4
Radiation type	Synchrotron X-ray, λ = 0.728243 Å	
Specimen shape, size (mm)	Cylinder, 1 × 0.5 × 0.7	
Data collection		
Diffractometer	SSRL beam line 2-1	
Specimen mounting	Kapton capillary	
Data collection mode	Transmission	
Scan method	Step	
2θ values (°)	$2\theta_{min}$ = 9 $2\theta_{max}$ = 116 $2\theta_{step}$ = 0.005	
Refinement		
R factors and goodness of fit (G.O.F.)	R_p = 0.035, R_{wp} = 0.053, R_{exp} = 0.237, χ^2 = 0.050, G.O.F. = 0.22	
No. of parameters	30	
No. of restraints	0	

Table S2. Fractional atomic coordinates and isotropic or equivalent isotropic displacement parameters (Å^2) for $Ca_{0.65}Ce_{0.35}Ti_{0.3}Mn_{0.7}O_3$.

	x	*y*	*z*	B_{iso}*/B_{eq}	Occ. (<1)
Ca1	0.05926 (8)	0.25	−0.01056 (14)	0.10684	0.65
Ce2	0.05926 (8)	0.25	−0.01056 (14)	0.10684	0.35
Ti3	0	0	0.5	0.10684	0.3
Mn4	0	0	0.5	0.10684	0.7
O5	0.4724 (5)	0.25	0.0926 (5)	0.10 (3)	1
O6	0.1913 (4)	0.5476 (3)	0.2041 (4)	0.10 (3)	1

Table S3. Geometric parameters (Å, °) for $Ca_{0.65}Ce_{0.35}Ti_{0.3}Mn_{0.7}O_3$.

Ca1—Ce2	-	Mn4—O6^{i}	2.080 (2)
Ca1—O5^{i}	2.291 (3)	Mn4—O6^{xii}	2.080 (2)
Ca1—O6^{ii}	2.322 (2)	Mn4—Ca1^{xi}	3.1137 (3)
Ca1—O6^{iii}	2.322 (2)	Mn4—Ce2^{i}	3.1137 (3)
Ca1—O5	2.385 (3)	Mn4—Ca1^{i}	3.1137 (3)
Ca1—O6^{iv}	2.576 (2)	Mn4—Ce2^{xi}	3.1137 (3)
Ca1—O6^{v}	2.576 (2)	O5—Ti3^{viii}	1.9593 (8)
Ca1—O6^{vi}	2.632 (2)	O5—Mn4^{viii}	1.9593 (8)
Ca1—O6	2.632 (2)	O5—Ti3^{vii}	1.9593 (8)
Ca1—Mn4^{vii}	3.1137 (3)	O5—Mn4^{vii}	1.9593 (8)
Ca1—Ti3^{vii}	3.1137 (3)	O5—Ca1^{xiii}	2.291 (3)
Ca1—Mn4^{viii}	3.1137 (3)	O5—Ce2^{xiii}	2.291 (3)
Ca1—Ti3^{viii}	3.1137 (3)	O5—Ca1	2.385 (3)
Ca1—O5^{ix}	3.155 (3)	O5—Ce2	2.385 (3)
Ce2—Ca1	-	O5—O6^{v}	2.741 (3)
Ce2—O5^{i}	2.291 (3)	O5—O6^{iv}	2.741 (3)

Ce2—O6^{ii}	2.322 (2)	O5—O6^{xiii}	2.784 (3)
Ce2—O6^{iii}	2.322 (2)	O5—O6^{xiv}	2.784 (3)
Ce2—O5	2.385 (3)	O5—O6	2.812 (3)
Ce2—O6^{iv}	2.576 (2)	O5—O6^{vi}	2.812 (3)
Ce2—O6^{v}	2.576 (2)	O5—O6^{xv}	2.903 (3)
Ce2—O6^{vi}	2.632 (2)	O5—O6^{xvi}	2.903 (3)
Ce2—O6	2.632 (2)	O5—Ca1^{xvii}	3.155 (3)
Ce2—Mn4^{vii}	3.1137 (3)	O5—Ce2^{xvii}	3.155 (3)
Ce2—Ti3^{vii}	3.1137 (3)	O6—Mn4^{xviii}	1.948 (2)
Ce2—Mn4^{viii}	3.1137 (3)	O6—Ti3^{xviii}	1.948 (2)
Ce2—Ti3^{viii}	3.1137 (3)	O6—Mn4^{viii}	2.080 (2)
Ce2—O5^{ix}	3.155 (3)	O6—Ti3^{viii}	2.080 (2)
Ti3—Mn4	-	O6—Ca1^{xix}	2.322 (2)
Ti3—O6^{x}	1.948 (2)	O6—Ce2^{xix}	2.322 (2)
Ti3—O6^{vi}	1.948 (2)	O6—Ca1^{xx}	2.576 (2)
Ti3—O5^{xi}	1.9593 (8)	O6—Ce2^{xx}	2.576 (2)
Ti3—O5^{i}	1.9593 (8)	O6—Ce2	2.632 (2)
Ti3—O6^{i}	2.080 (2)	O6—Ca1	2.632 (2)
Ti3—O6^{xii}	2.080 (2)	O6—O5^{xx}	2.741 (3)
Ti3—Ca1^{xi}	3.1137 (3)	O6—O5^{i}	2.784 (3)
Ti3—Ce2^{i}	3.1137 (3)	O6—O5	2.812 (3)
Ti3—Ca1^{i}	3.1137 (3)	O6—O6^{xx}	2.8498 (16)
Ti3—Ce2^{xi}	3.1137 (3)	O6—O6^{v}	2.8498 (16)
Mn4—Ti3	-	O6—O6^{xxi}	2.8500 (6)
Mn4—O6^{x}	1.948 (2)	O6—O6^{xiv}	2.8500 (6)
Mn4—O6^{vi}	1.948 (2)	O6—O5^{xxii}	2.903 (3)

Mn4—O5^{xi}	1.9593 (8)	O6—O6^{xxiii}	3.059 (5)
Mn4—O5^{i}	1.9593 (8)	O6—O6^{ii}	3.148 (5)
O5^{i}—Ca1—Ce2	-	Ce2—O5—Mn4^{viii}	91.04 (9)
O6^{ii}—Ca1—O5^{i}	107.89 (8)	Ce2—O5—Ti3^{viii}	91.04 (9)
O6^{ii}—Ca1—Ce2	-	O6^{v}—O5—Ce2	59.86 (8)
O6^{iii}—Ca1—O6^{ii}	82.39 (11)	O6^{v}—O5—Ca1	59.86 (8)
O6^{iii}—Ca1—O5^{i}	107.89 (8)	O6^{v}—O5—Ce2^{xiii}	144.40 (7)
O6^{iii}—Ca1—Ce2	-	O6^{v}—O5—Ca1^{xiii}	144.40 (7)
O5—Ca1—O6^{iii}	133.85 (6)	O6^{v}—O5—Mn4^{vii}	111.86 (13)
O5—Ca1—O6^{ii}	133.85 (6)	O6^{v}—O5—Ti3^{vii}	111.86 (13)
O5—Ca1—O5^{i}	88.89 (8)	O6^{v}—O5—Mn4^{viii}	45.28 (7)
O5—Ca1—Ce2	-	O6^{v}—O5—Ti3^{viii}	45.28 (7)
O6^{iv}—Ca1—O5	66.96 (7)	O6^{iv}—O5—O6^{v}	67.83 (12)
O6^{iv}—Ca1—O6^{iii}	70.95 (5)	O6^{iv}—O5—Ce2	59.86 (8)
O6^{iv}—Ca1—O6^{ii}	117.11 (5)	O6^{iv}—O5—Ca1	59.86 (8)
O6^{iv}—Ca1—O5^{i}	134.06 (7)	O6^{iv}—O5—Ce2^{xiii}	144.40 (7)
O6^{iv}—Ca1—Ce2	-	O6^{iv}—O5—Ca1^{xiii}	144.40 (7)
O6^{v}—Ca1—O6^{iv}	72.84 (10)	O6^{iv}—O5—Mn4^{vii}	45.28 (7)
O6^{v}—Ca1—O5	66.96 (7)	O6^{iv}—O5—Ti3^{vii}	45.28 (7)
O6^{v}—Ca1—O6^{iii}	117.11 (5)	O6^{iv}—O5—Mn4^{viii}	111.86 (13)
O6^{v}—Ca1—O6^{ii}	70.95 (5)	O6^{iv}—O5—Ti3^{viii}	111.86 (13)
O6^{v}—Ca1—O5^{i}	134.06 (7)	O6^{xiii}—O5—O6^{iv}	89.67 (7)
O6^{v}—Ca1—Ce2	-	O6^{xiii}—O5—O6^{v}	153.57 (11)
O6^{vi}—Ca1—O6^{v}	127.82 (4)	O6^{xiii}—O5—Ce2	121.33 (7)
O6^{vi}—Ca1—O6^{iv}	66.34 (3)	O6^{xiii}—O5—Ca1	121.33 (7)

O6^{vi}—Ca1—O5	67.97 (6)	O6^{xiii}—O5—Ce2^{xiii}	61.57 (7)
O6^{vi}—Ca1—O6^{iii}	78.62 (8)	O6^{xiii}—O5—Ca1^{xiii}	61.57 (7)
O6^{vi}—Ca1—O6^{ii}	158.16 (6)	O6^{xiii}—O5—Mn4^{vii}	44.38 (6)
O6^{vi}—Ca1—O5^{i}	68.49 (6)	O6^{xiii}—O5—Ti3^{vii}	44.38 (6)
O6^{vi}—Ca1—Ce2	-	O6^{xiii}—O5—Mn4^{viii}	147.44 (14)
O6—Ca1—O6^{vi}	117.39 (10)	O6^{xiii}—O5—Ti3^{viii}	147.44 (14)
O6—Ca1—O6^{v}	66.34 (3)	O6^{xiv}—O5—O6^{xiii}	107.74 (13)
O6—Ca1—O6^{iv}	127.82 (4)	O6^{xiv}—O5—O6^{iv}	153.57 (11)
O6—Ca1—O5	67.97 (6)	O6^{xiv}—O5—O6^{v}	89.67 (7)
O6—Ca1—O6^{iii}	158.16 (6)	O6^{xiv}—O5—Ce2	121.33 (7)
O6—Ca1—O6^{ii}	78.62 (8)	O6^{xiv}—O5—Ca1	121.33 (7)
O6—Ca1—O5^{i}	68.49 (6)	O6^{xiv}—O5—Ce2^{xiii}	61.57 (7)
O6—Ca1—Ce2	-	O6^{xiv}—O5—Ca1^{xiii}	61.57 (7)
Mn4^{vii}—Ca1—O6	106.66 (5)	O6^{xiv}—O5—Mn4^{vii}	147.44 (14)
Mn4^{vii}—Ca1—O6^{vi}	41.40 (5)	O6^{xiv}—O5—Ti3^{vii}	147.44 (14)
Mn4^{vii}—Ca1—O6^{v}	86.50 (5)	O6^{xiv}—O5—Mn4^{viii}	44.38 (6)
Mn4^{vii}—Ca1—O6^{iv}	38.60 (5)	O6^{xiv}—O5—Ti3^{viii}	44.38 (6)
Mn4^{vii}—Ca1—O5	38.99 (2)	O6—O5—O6^{xiv}	61.23 (5)
Mn4^{vii}—Ca1—O6^{iii}	95.16 (6)	O6—O5—O6^{xiii}	144.17 (12)
Mn4^{vii}—Ca1—O6^{ii}	152.77 (6)	O6—O5—O6^{iv}	114.78 (11)
Mn4^{vii}—Ca1—O5^{i}	98.71 (6)	O6—O5—O6^{v}	61.74 (5)
Mn4^{vii}—Ca1—Ce2	-	O6—O5—Ce2	60.20 (7)
Ti3^{vii}—Ca1—Mn4^{vii}	0	O6—O5—Ca1	60.20 (7)
Ti3^{vii}—Ca1—O6	106.66 (5)	O6—O5—Ce2^{xiii}	84.95 (9)
Ti3^{vii}—Ca1—O6^{vi}	41.40 (5)	O6—O5—Ca1^{xiii}	84.95 (9)

Ti3^{vii}—Ca1—O6^{v}	86.50 (5)	O6—O5—Mn4^{vii}	150.38 (14)
Ti3^{vii}—Ca1—O6^{iv}	38.60 (5)	O6—O5—Ti3^{vii}	150.38 (14)
Ti3^{vii}—Ca1—O5	38.99 (2)	O6—O5—Mn4^{viii}	47.69 (6)
Ti3^{vii}—Ca1—O6^{iii}	95.16 (6)	O6—O5—Ti3^{viii}	47.69 (6)
Ti3^{vii}—Ca1—O6^{ii}	152.77 (6)	O6^{vi}—O5—O6	106.23 (13)
Ti3^{vii}—Ca1—O5^{i}	98.71 (6)	O6^{vi}—O5—O6^{xiv}	144.17 (12)
Ti3^{vii}—Ca1—Ce2	-	O6^{vi}—O5—O6^{xiii}	61.23 (5)
Mn4^{viii}—Ca1—Ti3^{vii}	74.705 (10)	O6^{vi}—O5—O6^{iv}	61.74 (5)
Mn4^{viii}—Ca1—Mn4^{vii}	74.705 (10)	O6^{vi}—O5—O6^{v}	114.78 (11)
Mn4^{viii}—Ca1—O6	41.40 (5)	O6^{vi}—O5—Ce2	60.20 (7)
Mn4^{viii}—Ca1—O6^{vi}	106.66 (5)	O6^{vi}—O5—Ca1	60.20 (7)
Mn4^{viii}—Ca1—O6^{v}	38.60 (5)	O6^{vi}—O5—Ce2^{xiii}	84.95 (9)
Mn4^{viii}—Ca1—O6^{iv}	86.50 (5)	O6^{vi}—O5—Ca1^{xiii}	84.95 (9)
Mn4^{viii}—Ca1—O5	38.99 (2)	O6^{vi}—O5—Mn4^{vii}	47.69 (6)
Mn4^{viii}—Ca1—O6^{iii}	152.77 (6)	O6^{vi}—O5—Ti3^{vii}	47.69 (6)
Mn4^{viii}—Ca1—O6^{ii}	95.16 (6)	O6^{vi}—O5—Mn4^{viii}	150.38 (14)
Mn4^{viii}—Ca1—O5^{i}	98.71 (6)	O6^{vi}—O5—Ti3^{viii}	150.38 (14)
Mn4^{viii}—Ca1—Ce2	-	O6^{xv}—O5—O6^{vi}	93.43 (7)
Ti3^{viii}—Ca1—Mn4^{viii}	0	O6^{xv}—O5—O6	154.51 (11)
Ti3^{viii}—Ca1—Ti3^{vii}	74.705 (10)	O6^{xv}—O5—O6^{xiv}	110.64 (10)
Ti3^{viii}—Ca1—Mn4^{vii}	74.705 (10)	O6^{xv}—O5—O6^{xiii}	60.10 (5)
Ti3^{viii}—Ca1—O6	41.40 (5)	O6^{xv}—O5—O6^{iv}	60.58 (6)
Ti3^{viii}—Ca1—O6^{vi}	106.66 (5)	O6^{xv}—O5—O6^{v}	95.55 (10)
Ti3^{viii}—Ca1—O6^{v}	38.60 (5)	O6^{xv}—O5—Ce2	120.39 (10)
Ti3^{viii}—Ca1—O6^{iv}	86.50 (5)	O6^{xv}—O5—Ca1	120.39 (10)

Ti3^{viii}—Ca1—O5	38.99 (2)	O6^{xv}—O5—Ce2^{xiii}	113.35 (10)
Ti3^{viii}—Ca1—O6^{iii}	152.77 (6)	O6^{xv}—O5—Ca1^{xiii}	113.35 (10)
Ti3^{viii}—Ca1—O6^{ii}	95.16 (6)	O6^{xv}—O5—Mn4^{vii}	45.74 (7)
Ti3^{viii}—Ca1—O5^{i}	98.71 (6)	O6^{xv}—O5—Ti3^{vii}	45.74 (7)
Ti3^{viii}—Ca1—Ce2	-	O6^{xv}—O5—Mn4^{viii}	108.55 (12)
O5^{ix}—Ca1—Ti3^{viii}	98.09 (4)	O6^{xv}—O5—Ti3^{viii}	108.55 (12)
O5^{ix}—Ca1—Mn4^{viii}	98.09 (4)	O6^{xvi}—O5—O6^{xv}	63.58 (11)
O5^{ix}—Ca1—Ti3^{vii}	98.09 (4)	O6^{xvi}—O5—O6^{vi}	154.51 (11)
O5^{ix}—Ca1—Mn4^{vii}	98.09 (4)	O6^{xvi}—O5—O6	93.43 (7)
O5^{ix}—Ca1—O6	118.36 (5)	O6^{xvi}—O5—O6^{xiv}	60.10 (5)
O5^{ix}—Ca1—O6^{vi}	118.36 (5)	O6^{xvi}—O5—O6^{xiii}	110.64 (10)
O5^{ix}—Ca1—O6^{v}	59.86 (7)	O6^{xvi}—O5—O6^{iv}	95.55 (10)
O5^{ix}—Ca1—O6^{iv}	59.86 (7)	O6^{xvi}—O5—O6^{v}	60.58 (6)
O5^{ix}—Ca1—O5	112.28 (9)	O6^{xvi}—O5—Ce2	120.39 (10)
O5^{ix}—Ca1—O6^{iii}	57.69 (7)	O6^{xvi}—O5—Ca1	120.39 (10)
O5^{ix}—Ca1—O6^{ii}	57.69 (7)	O6^{xvi}—O5—Ce2^{xiii}	113.35 (10)
O5^{ix}—Ca1—O5^{i}	158.82 (12)	O6^{xvi}—O5—Ca1^{xiii}	113.35 (10)
O5^{ix}—Ca1—Ce2	-	O6^{xvi}—O5—Mn4^{vii}	108.55 (12)
O5^{i}—Ce2—Ca1	-	O6^{xvi}—O5—Ti3^{vii}	108.55 (12)
O6^{ii}—Ce2—O5^{i}	107.89 (8)	O6^{xvi}—O5—Mn4^{viii}	45.74 (7)
O6^{ii}—Ce2—Ca1	-	O6^{xvi}—O5—Ti3^{viii}	45.74 (7)
O6^{iii}—Ce2—O6^{ii}	82.39 (11)	Ca1^{xvii}—O5—O6^{xvi}	50.12 (6)
O6^{iii}—Ce2—O5^{i}	107.89 (8)	Ca1^{xvii}—O5—O6^{xv}	50.12 (6)
O6^{iii}—Ce2—Ca1	-	Ca1^{xvii}—O5—O6^{vi}	107.25 (8)
O5—Ce2—O6^{iii}	133.85 (6)	Ca1^{xvii}—O5—O6	107.25 (8)

O5—Ce2—O6^{ii}	133.85 (6)	Ca1^{xvii}—O5—O6^{xiv}	108.55 (8)
O5—Ce2—O5^{i}	88.89 (8)	Ca1^{xvii}—O5—O6^{xiii}	108.55 (8)
O5—Ce2—Ca1	-	Ca1^{xvii}—O5—O6^{iv}	45.72 (6)
O6^{iv}—Ce2—O5	66.96 (7)	Ca1^{xvii}—O5—O6^{v}	45.72 (6)
O6^{iv}—Ce2—O6^{iii}	70.95 (5)	Ca1^{xvii}—O5—Ce2	85.50 (9)
O6^{iv}—Ce2—O6^{ii}	117.11 (5)	Ca1^{xvii}—O5—Ca1	85.50 (9)
O6^{iv}—Ce2—O5^{i}	134.06 (7)	Ca1^{xvii}—O5—Ce2^{xiii}	158.82 (12)
O6^{iv}—Ce2—Ca1	-	Ca1^{xvii}—O5—Ca1^{xiii}	158.82 (12)
O6^{v}—Ce2—O6^{iv}	72.84 (10)	Ca1^{xvii}—O5—Mn4^{vii}	74.80 (8)
O6^{v}—Ce2—O5	66.96 (7)	Ca1^{xvii}—O5—Ti3^{vii}	74.80 (8)
O6^{v}—Ce2—O6^{iii}	117.11 (5)	Ca1^{xvii}—O5—Mn4^{viii}	74.80 (8)
O6^{v}—Ce2—O6^{ii}	70.95 (5)	Ca1^{xvii}—O5—Ti3^{viii}	74.80 (8)
O6^{v}—Ce2—O5^{i}	134.06 (7)	Ce2^{xvii}—O5—Ca1^{xvii}	0
O6^{v}—Ce2—Ca1	-	Ce2^{xvii}—O5—O6^{xvi}	50.12 (6)
O6^{vi}—Ce2—O6^{v}	127.82 (4)	Ce2^{xvii}—O5—O6^{xv}	50.12 (6)
O6^{vi}—Ce2—O6^{iv}	66.34 (3)	Ce2^{xvii}—O5—O6^{vi}	107.25 (8)
O6^{vi}—Ce2—O5	67.97 (6)	Ce2^{xvii}—O5—O6	107.25 (8)
O6^{vi}—Ce2—O6^{iii}	78.62 (8)	Ce2^{xvii}—O5—O6^{xiv}	108.55 (8)
O6^{vi}—Ce2—O6^{ii}	158.16 (6)	Ce2^{xvii}—O5—O6^{xiii}	108.55 (8)
O6^{vi}—Ce2—O5^{i}	68.49 (6)	Ce2^{xvii}—O5—O6^{iv}	45.72 (6)
O6^{vi}—Ce2—Ca1	-	Ce2^{xvii}—O5—O6^{v}	45.72 (6)
O6—Ce2—O6^{vi}	117.39 (10)	Ce2^{xvii}—O5—Ce2	85.50 (9)
O6—Ce2—O6^{v}	66.34 (3)	Ce2^{xvii}—O5—Ca1	85.50 (9)
O6—Ce2—O6^{iv}	127.82 (4)	Ce2^{xvii}—O5—Ce2^{xiii}	158.82 (12)
O6—Ce2—O5	67.97 (6)	Ce2^{xvii}—O5—Ca1^{xiii}	158.82 (12)

O6—Ce2—O6^{iii}	158.16 (6)	Ce2^{xvii}—O5—Mn4^{vii}	74.80 (8)
O6—Ce2—O6^{ii}	78.62 (8)	Ce2^{xvii}—O5—Ti3^{vii}	74.80 (8)
O6—Ce2—O5^{i}	68.49 (6)	Ce2^{xvii}—O5—Mn4^{viii}	74.80 (8)
O6—Ce2—Ca1	-	Ce2^{xvii}—O5—Ti3^{viii}	74.80 (8)
Mn4^{vii}—Ce2—O6	106.66 (5)	Ti3^{xviii}—O6—Mn4^{xviii}	0
Mn4^{vii}—Ce2—O6^{vi}	41.40 (5)	Mn4^{viii}—O6—Ti3^{xviii}	148.74 (12)
Mn4^{vii}—Ce2—O6^{v}	86.50 (5)	Mn4^{viii}—O6—Mn4^{xviii}	148.74 (12)
Mn4^{vii}—Ce2—O6^{iv}	38.60 (5)	Ti3^{viii}—O6—Mn4^{viii}	0
Mn4^{vii}—Ce2—O5	38.99 (2)	Ti3^{viii}—O6—Ti3^{xviii}	148.74 (12)
Mn4^{vii}—Ce2—O6^{iii}	95.16 (6)	Ti3^{viii}—O6—Mn4^{xviii}	148.74 (12)
Mn4^{vii}—Ce2—O6^{ii}	152.77 (6)	Ca1^{xix}—O6—Ti3^{viii}	112.59 (10)
Mn4^{vii}—Ce2—O5^{i}	98.71 (6)	Ca1^{xix}—O6—Mn4^{viii}	112.59 (10)
Mn4^{vii}—Ce2—Ca1	-	Ca1^{xix}—O6—Ti3^{xviii}	98.67 (9)
Ti3^{vii}—Ce2—Mn4^{vii}	0	Ca1^{xix}—O6—Mn4^{xviii}	98.67 (9)
Ti3^{vii}—Ce2—O6	106.66 (5)	Ce2^{xix}—O6—Ca1^{xix}	0
Ti3^{vii}—Ce2—O6^{vi}	41.40 (5)	Ce2^{xix}—O6—Ti3^{viii}	112.59 (10)
Ti3^{vii}—Ce2—O6^{v}	86.50 (5)	Ce2^{xix}—O6—Mn4^{viii}	112.59 (10)
Ti3^{vii}—Ce2—O6^{iv}	38.60 (5)	Ce2^{xix}—O6—Ti3^{xviii}	98.67 (9)
Ti3^{vii}—Ce2—O5	38.99 (2)	Ce2^{xix}—O6—Mn4^{xviii}	98.67 (9)
Ti3^{vii}—Ce2—O6^{iii}	95.16 (6)	Ca1^{xx}—O6—Ce2^{xix}	101.72 (9)
Ti3^{vii}—Ce2—O6^{ii}	152.77 (6)	Ca1^{xx}—O6—Ca1^{xix}	101.72 (9)
Ti3^{vii}—Ce2—O5^{i}	98.71 (6)	Ca1^{xx}—O6—Ti3^{viii}	87.79 (8)
Ti3^{vii}—Ce2—Ca1	-	Ca1^{xx}—O6—Mn4^{viii}	87.79 (8)
Mn4^{viii}—Ce2—Ti3^{vii}	74.705 (10)	Ca1^{xx}—O6—Ti3^{xviii}	85.80 (8)
Mn4^{viii}—Ce2—Mn4^{vii}	74.705 (10)	Ca1^{xx}—O6—Mn4^{xviii}	85.80 (8)

Mn4^{viii}—Ce2—O6	41.40 (5)	Ce2^{xx}—O6—Ca1^{xx}	0
Mn4^{viii}—Ce2—O6^{vi}	106.66 (5)	Ce2^{xx}—O6—Ce2^{xix}	101.72 (9)
Mn4^{viii}—Ce2—O6^{v}	38.60 (5)	Ce2^{xx}—O6—Ca1^{xix}	101.72 (9)
Mn4^{viii}—Ce2—O6^{iv}	86.50 (5)	Ce2^{xx}—O6—Ti3^{viii}	87.79 (8)
Mn4^{viii}—Ce2—O5	38.99 (2)	Ce2^{xx}—O6—Mn4^{viii}	87.79 (8)
Mn4^{viii}—Ce2—O6^{iii}	152.77 (6)	Ce2^{xx}—O6—Ti3^{xviii}	85.80 (8)
Mn4^{viii}—Ce2—O6^{ii}	95.16 (6)	Ce2^{xx}—O6—Mn4^{xviii}	85.80 (8)
Mn4^{viii}—Ce2—O5^{i}	98.71 (6)	Ce2—O6—Ce2^{xx}	156.84 (9)
Mn4^{viii}—Ce2—Ca1	-	Ce2—O6—Ca1^{xx}	156.84 (9)
Ti3^{viii}—Ce2—Mn4^{viii}	0	Ce2—O6—Ce2^{xix}	101.38 (8)
Ti3^{viii}—Ce2—Ti3^{vii}	74.705 (10)	Ce2—O6—Ca1^{xix}	101.38 (8)
Ti3^{viii}—Ce2—Mn4^{vii}	74.705 (10)	Ce2—O6—Ti3^{viii}	81.81 (8)
Ti3^{viii}—Ce2—O6	41.40 (5)	Ce2—O6—Mn4^{viii}	81.81 (8)
Ti3^{viii}—Ce2—O6^{vi}	106.66 (5)	Ce2—O6—Ti3^{xviii}	92.42 (9)
Ti3^{viii}—Ce2—O6^{v}	38.60 (5)	Ce2—O6—Mn4^{xviii}	92.42 (9)
Ti3^{viii}—Ce2—O6^{iv}	86.50 (5)	Ca1—O6—Ce2	0
Ti3^{viii}—Ce2—O5	38.99 (2)	Ca1—O6—Ce2^{xx}	156.84 (9)
Ti3^{viii}—Ce2—O6^{iii}	152.77 (6)	Ca1—O6—Ca1^{xx}	156.84 (9)
Ti3^{viii}—Ce2—O6^{ii}	95.16 (6)	Ca1—O6—Ce2^{xix}	101.38 (8)
Ti3^{viii}—Ce2—O5^{i}	98.71 (6)	Ca1—O6—Ca1^{xix}	101.38 (8)
Ti3^{viii}—Ce2—Ca1	-	Ca1—O6—Ti3^{viii}	81.81 (8)
O5^{ix}—Ce2—Ti3^{viii}	98.09 (4)	Ca1—O6—Mn4^{viii}	81.81 (8)
O5^{ix}—Ce2—Mn4^{viii}	98.09 (4)	Ca1—O6—Ti3^{xviii}	92.42 (9)
O5^{ix}—Ce2—Ti3^{vii}	98.09 (4)	Ca1—O6—Mn4^{xviii}	92.42 (9)
O5^{ix}—Ce2—Mn4^{vii}	98.09 (4)	O5^{xx}—O6—Ca1	135.54 (10)

O5^{ix}—Ce2—O6	118.36 (5)	O5^{xx}—O6—Ce2	135.54 (10)
O5^{ix}—Ce2—O6^{vi}	118.36 (5)	O5^{xx}—O6—Ce2^{xx}	53.18 (7)
O5^{ix}—Ce2—O6^{v}	59.86 (7)	O5^{xx}—O6—Ca1^{xx}	53.18 (7)
O5^{ix}—Ce2—O6^{iv}	59.86 (7)	O5^{xx}—O6—Ce2^{xix}	76.59 (8)
O5^{ix}—Ce2—O5	112.28 (9)	O5^{xx}—O6—Ca1^{xix}	76.59 (8)
O5^{ix}—Ce2—O6^{iii}	57.69 (7)	O5^{xx}—O6—Ti3^{viii}	140.78 (11)
O5^{ix}—Ce2—O6^{ii}	57.69 (7)	O5^{xx}—O6—Mn4^{viii}	140.78 (11)
O5^{ix}—Ce2—O5^{i}	158.82 (12)	O5^{xx}—O6—Ti3^{xviii}	45.62 (6)
O5^{ix}—Ce2—Ca1	-	O5^{xx}—O6—Mn4^{xviii}	45.62 (6)
O6^{x}—Ti3—Mn4	-	O5^{i}—O6—O5^{xx}	90.33 (7)
O6^{vi}—Ti3—O6^{x}	180.0000 (1)	O5^{i}—O6—Ca1	49.94 (7)
O6^{vi}—Ti3—Mn4	-	O5^{i}—O6—Ce2	49.94 (7)
O5^{xi}—Ti3—O6^{vi}	89.10 (11)	O5^{i}—O6—Ce2^{xx}	119.17 (11)
O5^{xi}—Ti3—O6^{x}	90.90 (11)	O5^{i}—O6—Ca1^{xx}	119.17 (11)
O5^{xi}—Ti3—Mn4	-	O5^{i}—O6—Ce2^{xix}	116.05 (10)
O5^{i}—Ti3—O5^{xi}	180	O5^{i}—O6—Ca1^{xix}	116.05 (10)
O5^{i}—Ti3—O6^{vi}	90.90 (11)	O5^{i}—O6—Ti3^{viii}	115.69 (10)
O5^{i}—Ti3—O6^{x}	89.10 (11)	O5^{i}—O6—Mn4^{viii}	115.69 (10)
O5^{i}—Ti3—Mn4	-	O5^{i}—O6—Ti3^{xviii}	44.71 (7)
O6^{i}—Ti3—O5^{i}	88.17 (10)	O5^{i}—O6—Mn4^{xviii}	44.71 (7)
O6^{i}—Ti3—O5^{xi}	91.83 (10)	O5—O6—O5^{i}	71.62 (7)
O6^{i}—Ti3—O6^{vi}	90.00 (3)	O5—O6—O5^{xx}	142.73 (13)
O6^{i}—Ti3—O6^{x}	90.00 (3)	O5—O6—Ca1	51.83 (7)
O6^{i}—Ti3—Mn4	-	O5—O6—Ce2	51.83 (7)
O6^{xii}—Ti3—O6^{i}	180	O5—O6—Ce2^{xx}	107.20 (9)

O6^{xii}—Ti3—O5^{i}	91.83 (10)	O5—O6—Ca1^{xx}	107.20 (9)
O6^{xii}—Ti3—O5^{xi}	88.17 (10)	O5—O6—Ce2^{xix}	140.55 (12)
O6^{xii}—Ti3—O6^{vi}	90.00 (3)	O5—O6—Ca1^{xix}	140.55 (12)
O6^{xii}—Ti3—O6^{x}	90.00 (3)	O5—O6—Ti3^{viii}	44.15 (6)
O6^{xii}—Ti3—Mn4	-	O5—O6—Mn4^{viii}	44.15 (6)
Ca1^{xi}—Ti3—O6^{xii}	56.79 (6)	O5—O6—Ti3^{xviii}	109.54 (11)
Ca1^{xi}—Ti3—O6^{i}	123.21 (6)	O5—O6—Mn4^{xviii}	109.54 (11)
Ca1^{xi}—Ti3—O5^{i}	130.03 (8)	O6^{xx}—O6—O5	82.40 (12)
Ca1^{xi}—Ti3—O5^{xi}	49.97 (8)	O6^{xx}—O6—O5^{i}	62.01 (10)
Ca1^{xi}—Ti3—O6^{vi}	55.60 (7)	O6^{xx}—O6—O5^{xx}	60.35 (7)
Ca1^{xi}—Ti3—O6^{x}	124.40 (7)	O6^{xx}—O6—Ca1	105.05 (12)
Ca1^{xi}—Ti3—Mn4	-	O6^{xx}—O6—Ce2	105.05 (12)
Ce2^{i}—Ti3—Ca1^{xi}	180.0000 (1)	O6^{xx}—O6—Ce2^{xx}	57.78 (7)
Ce2^{i}—Ti3—O6^{xii}	123.21 (6)	O6^{xx}—O6—Ca1^{xx}	57.78 (7)
Ce2^{i}—Ti3—O6^{i}	56.79 (6)	O6^{xx}—O6—Ce2^{xix}	136.53 (12)
Ce2^{i}—Ti3—O5^{i}	49.97 (8)	O6^{xx}—O6—Ca1^{xix}	136.53 (12)
Ce2^{i}—Ti3—O5^{xi}	130.03 (8)	O6^{xx}—O6—Ti3^{viii}	104.90 (13)
Ce2^{i}—Ti3—O6^{vi}	124.40 (7)	O6^{xx}—O6—Mn4^{viii}	104.90 (13)
Ce2^{i}—Ti3—O6^{x}	55.60 (7)	O6^{xx}—O6—Ti3^{xviii}	46.88 (5)
Ce2^{i}—Ti3—Mn4	-	O6^{xx}—O6—Mn4^{xviii}	46.88 (5)
Ca1^{i}—Ti3—Ce2^{i}	0	O6^{v}—O6—O6^{xx}	139.95 (17)
Ca1^{i}—Ti3—Ca1^{xi}	180.0000 (1)	O6^{v}—O6—O5	57.91 (11)
Ca1^{i}—Ti3—O6^{xii}	123.21 (6)	O6^{v}—O6—O5^{i}	105.40 (13)
Ca1^{i}—Ti3—O6^{i}	56.79 (6)	O6^{v}—O6—O5^{xx}	158.69 (13)
Ca1^{i}—Ti3—O5^{i}	49.97 (8)	O6^{v}—O6—Ca1	55.89 (8)

$Ca1^{i}$—Ti3—$O5^{xi}$	130.03 (8)	$O6^{v}$—O6—Ce2	55.89 (8)
$Ca1^{i}$—Ti3—$O6^{vi}$	124.40 (7)	$O6^{v}$—O6—$Ce2^{xx}$	125.56 (12)
$Ca1^{i}$—Ti3—$O6^{x}$	55.60 (7)	$O6^{v}$—O6—$Ca1^{xx}$	125.56 (12)
$Ca1^{i}$—Ti3—Mn4	-	$O6^{v}$—O6—$Ce2^{xix}$	83.52 (8)
$Ce2^{xi}$—Ti3—$Ca1^{i}$	180.0000 (1)	$O6^{v}$—O6—$Ca1^{xix}$	83.52 (8)
$Ce2^{xi}$—Ti3—$Ce2^{i}$	180.0000 (1)	$O6^{v}$—O6—$Ti3^{viii}$	43.12 (7)
$Ce2^{xi}$—Ti3—$Ca1^{xi}$	0	$O6^{v}$—O6—$Mn4^{viii}$	43.12 (7)
$Ce2^{xi}$—Ti3—$O6^{xii}$	56.79 (6)	$O6^{v}$—O6—$Ti3^{xviii}$	147.70 (16)
$Ce2^{xi}$—Ti3—$O6^{i}$	123.21 (6)	$O6^{v}$—O6—$Mn4^{xviii}$	147.70 (16)
$Ce2^{xi}$—Ti3—$O5^{i}$	130.03 (8)	$O6^{xxi}$—O6—$O6^{v}$	112.95 (12)
$Ce2^{xi}$—Ti3—$O5^{xi}$	49.97 (8)	$O6^{xxi}$—O6—$O6^{xx}$	93.76 (12)
$Ce2^{xi}$—Ti3—$O6^{vi}$	55.60 (7)	$O6^{xxi}$—O6—O5	126.13 (7)
$Ce2^{xi}$—Ti3—$O6^{x}$	124.40 (7)	$O6^{xxi}$—O6—$O5^{i}$	59.86 (7)
$Ce2^{xi}$—Ti3—Mn4	-	$O6^{xxi}$—O6—$O5^{xx}$	62.52 (9)
$O6^{x}$—Mn4—Ti3	-	$O6^{xxi}$—O6—Ca1	78.34 (6)
$O6^{vi}$—Mn4—$O6^{x}$	180.0000 (1)	$O6^{xxi}$—O6—Ce2	78.34 (6)
$O6^{vi}$—Mn4—Ti3	-	$O6^{xxi}$—O6—$Ce2^{xx}$	115.66 (10)
$O5^{xi}$—Mn4—$O6^{vi}$	89.10 (11)	$O6^{xxi}$—O6—$Ca1^{xx}$	115.66 (10)
$O5^{xi}$—Mn4—$O6^{x}$	90.90 (11)	$O6^{xxi}$—O6—$Ce2^{xix}$	58.69 (6)
$O5^{xi}$—Mn4—Ti3	-	$O6^{xxi}$—O6—$Ca1^{xix}$	58.69 (6)
$O5^{i}$—Mn4—$O5^{xi}$	180	$O6^{xxi}$—O6—$Ti3^{viii}$	155.69 (14)
$O5^{i}$—Mn4—$O6^{vi}$	90.90 (11)	$O6^{xxi}$—O6—$Mn4^{viii}$	155.69 (14)
$O5^{i}$—Mn4—$O6^{x}$	89.10 (11)	$O6^{xxi}$—O6—$Ti3^{xviii}$	46.88 (7)
$O5^{i}$—Mn4—Ti3	-	$O6^{xxi}$—O6—$Mn4^{xviii}$	46.88 (7)
$O6^{i}$—Mn4—$O5^{i}$	88.17 (10)	$O6^{xiv}$—O6—$O6^{xxi}$	160.12 (19)

O6^{i}—Mn4—O5^{xi}	91.83 (10)	O6^{xiv}—O6—O6^{v}	86.24 (12)
O6^{i}—Mn4—O6^{vi}	90.00 (3)	O6^{xiv}—O6—O6^{xx}	67.05 (12)
O6^{i}—Mn4—O6^{x}	90.00 (3)	O6^{xiv}—O6—O5	58.92 (7)
O6^{i}—Mn4—Ti3	-	O6^{xiv}—O6—O5^{i}	111.54 (9)
O6^{xii}—Mn4—O6^{i}	180	O6^{xiv}—O6—O5^{xx}	101.50 (12)
O6^{xii}—Mn4—O5^{i}	91.83 (10)	O6^{xiv}—O6—Ca1	110.66 (6)
O6^{xii}—Mn4—O5^{xi}	88.17 (10)	O6^{xiv}—O6—Ce2	110.66 (6)
O6^{xii}—Mn4—O6^{vi}	90.00 (3)	O6^{xiv}—O6—Ce2^{xx}	50.36 (7)
O6^{xii}—Mn4—O6^{x}	90.00 (3)	O6^{xiv}—O6—Ca1^{xx}	50.36 (7)
O6^{xii}—Mn4—Ti3	-	O6^{xiv}—O6—Ce2^{xix}	132.36 (8)
Ca1^{xi}—Mn4—O6^{xii}	56.79 (6)	O6^{xiv}—O6—Ca1^{xix}	132.36 (8)
Ca1^{xi}—Mn4—O6^{i}	123.21 (6)	O6^{xiv}—O6—Ti3^{viii}	43.12 (5)
Ca1^{xi}—Mn4—O5^{i}	130.03 (8)	O6^{xiv}—O6—Mn4^{viii}	43.12 (5)
Ca1^{xi}—Mn4—O5^{xi}	49.97 (8)	O6^{xiv}—O6—Ti3^{xviii}	113.75 (14)
Ca1^{xi}—Mn4—O6^{vi}	55.60 (7)	O6^{xiv}—O6—Mn4^{xviii}	113.75 (14)
Ca1^{xi}—Mn4—O6^{x}	124.40 (7)	O5^{xxii}—O6—O6^{xiv}	56.90 (8)
Ca1^{xi}—Mn4—Ti3	-	O5^{xxii}—O6—O6^{xxi}	137.31 (10)
Ce2^{i}—Mn4—Ca1^{xi}	180.0000 (1)	O5^{xxii}—O6—O6^{v}	57.89 (8)
Ce2^{i}—Mn4—O6^{xii}	123.21 (6)	O5^{xxii}—O6—O6^{xx}	119.79 (13)
Ce2^{i}—Mn4—O6^{i}	56.79 (6)	O5^{xxii}—O6—O5	86.57 (7)
Ce2^{i}—Mn4—O5^{i}	49.97 (8)	O5^{xxii}—O6—O5^{i}	157.90 (11)
Ce2^{i}—Mn4—O5^{xi}	130.03 (8)	O5^{xxii}—O6—O5^{xx}	109.85 (10)
Ce2^{i}—Mn4—O6^{vi}	124.40 (7)	O5^{xxii}—O6—Ca1	113.22 (9)
Ce2^{i}—Mn4—O6^{x}	55.60 (7)	O5^{xxii}—O6—Ce2	113.22 (9)
Ce2^{i}—Mn4—Ti3	-	O5^{xxii}—O6—Ce2^{xx}	70.02 (8)

Ca1^{i}—Mn4—Ce2^{i}	0	O5^{xxii}—O6—Ca1^{xx}	70.02 (8)
Ca1^{i}—Mn4—Ca1^{xi}	180.0000 (1)	O5^{xxii}—O6—Ce2^{xix}	78.63 (8)
Ca1^{i}—Mn4—O6^{xii}	123.21 (6)	O5^{xxii}—O6—Ca1^{xix}	78.63 (8)
Ca1^{i}—Mn4—O6^{i}	56.79 (6)	O5^{xxii}—O6—Ti3^{viii}	42.42 (5)
Ca1^{i}—Mn4—O5^{i}	49.97 (8)	O5^{xxii}—O6—Mn4^{viii}	42.42 (5)
Ca1^{i}—Mn4—O5^{xi}	130.03 (8)	O5^{xxii}—O6—Ti3^{xviii}	154.30 (11)
Ca1^{i}—Mn4—O6^{vi}	124.40 (7)	O5^{xxii}—O6—Mn4^{xviii}	154.30 (11)
Ca1^{i}—Mn4—O6^{x}	55.60 (7)	O6^{xxiii}—O6—O5^{xxii}	58.21 (5)
Ca1^{i}—Mn4—Ti3	-	O6^{xxiii}—O6—O6^{xiv}	90
Ce2^{xi}—Mn4—Ca1^{i}	180.0000 (1)	O6^{xxiii}—O6—O6^{xxi}	90
Ce2^{xi}—Mn4—Ce2^{i}	180.0000 (1)	O6^{xxiii}—O6—O6^{v}	104.62 (9)
Ce2^{xi}—Mn4—Ca1^{xi}	0	O6^{xxiii}—O6—O6^{xx}	104.62 (9)
Ce2^{xi}—Mn4—O6^{xii}	56.79 (6)	O6^{xxiii}—O6—O5	143.12 (6)
Ce2^{xi}—Mn4—O6^{i}	123.21 (6)	O6^{xxiii}—O6—O5^{i}	143.87 (7)
Ce2^{xi}—Mn4—O5^{i}	130.03 (8)	O6^{xxiii}—O6—O5^{xx}	56.08 (6)
Ce2^{xi}—Mn4—O5^{xi}	49.97 (8)	O6^{xxiii}—O6—Ca1	148.69 (5)
Ce2^{xi}—Mn4—O6^{vi}	55.60 (7)	O6^{xxiii}—O6—Ce2	148.69 (5)
Ce2^{xi}—Mn4—O6^{x}	124.40 (7)	O6^{xxiii}—O6—Ce2^{xx}	53.58 (5)
Ce2^{xi}—Mn4—Ti3	-	O6^{xxiii}—O6—Ca1^{xx}	53.58 (5)
Mn4^{viii}—O5—Ti3^{viii}	0	O6^{xxiii}—O6—Ce2^{xix}	48.80 (6)
Ti3^{vii}—O5—Mn4^{viii}	149.25 (16)	O6^{xxiii}—O6—Ca1^{xix}	48.80 (6)
Ti3^{vii}—O5—Ti3^{viii}	149.25 (16)	O6^{xxiii}—O6—Ti3^{viii}	99.96 (6)
Mn4^{vii}—O5—Ti3^{vii}	0	O6^{xxiii}—O6—Mn4^{viii}	99.96 (6)
Mn4^{vii}—O5—Mn4^{viii}	149.25 (16)	O6^{xxiii}—O6—Ti3^{xviii}	100.64 (7)
Mn4^{vii}—O5—Ti3^{viii}	149.25 (16)	O6^{xxiii}—O6—Mn4^{xviii}	100.64 (7)

Ca1^{xiii}—O5—Mn4^{vii}	103.32 (8)	O6^{ii}—O6—O6^{xxiii}	103.21 (8)
Ca1^{xiii}—O5—Ti3^{vii}	103.32 (8)	O6^{ii}—O6—O5^{xxii}	100.62 (11)
Ca1^{xiii}—O5—Mn4^{viii}	103.32 (8)	O6^{ii}—O6—O6^{xiv}	142.37 (15)
Ca1^{xiii}—O5—Ti3^{viii}	103.32 (8)	O6^{ii}—O6—O6^{xxi}	56.47 (7)
Ce2^{xiii}—O5—Ca1^{xiii}	0	O6^{ii}—O6—O6^{v}	56.48 (7)
Ce2^{xiii}—O5—Mn4^{vii}	103.32 (8)	O6^{ii}—O6—O6^{xx}	138.80 (17)
Ce2^{xiii}—O5—Ti3^{vii}	103.32 (8)	O6^{ii}—O6—O5	93.03 (11)
Ce2^{xiii}—O5—Mn4^{viii}	103.32 (8)	O6^{ii}—O6—O5^{i}	77.63 (10)
Ce2^{xiii}—O5—Ti3^{viii}	103.32 (8)	O6^{ii}—O6—O5^{xx}	115.20 (12)
Ca1—O5—Ce2^{xiii}	115.68 (12)	O6^{ii}—O6—Ca1	46.32 (6)
Ca1—O5—Ca1^{xiii}	115.68 (12)	O6^{ii}—O6—Ce2	46.32 (6)
Ca1—O5—Mn4^{vii}	91.04 (9)	O6^{ii}—O6—Ce2^{xx}	156.72 (13)
Ca1—O5—Ti3^{vii}	91.04 (9)	O6^{ii}—O6—Ca1^{xx}	156.72 (13)
Ca1—O5—Mn4^{viii}	91.04 (9)	O6^{ii}—O6—Ce2^{xix}	55.06 (7)
Ca1—O5—Ti3^{viii}	91.04 (9)	O6^{ii}—O6—Ca1^{xix}	55.06 (7)
Ce2—O5—Ca1	0	O6^{ii}—O6—Ti3^{viii}	99.45 (11)
Ce2—O5—Ce2^{xiii}	115.68 (12)	O6^{ii}—O6—Mn4^{viii}	99.45 (11)
Ce2—O5—Ca1^{xiii}	115.68 (12)	O6^{ii}—O6—Ti3^{xviii}	98.42 (11)
Ce2—O5—Mn4^{vii}	91.04 (9)	O6^{ii}—O6—Mn4^{xviii}	98.42 (11)
Ce2—O5—Ti3^{vii}	91.04 (9)		

Symmetry codes: (i) x−1/2, −y+1/2, −z+1/2; (ii) −x, −y+1, −z; (iii) −x, y−1/2, −z; (iv) −x+1/2, y−1/2, z−1/2; (v) −x+1/2, −y+1, z−1/2; (vi) x, −y+1/2, z; (vii) −x+1/2, −y, z−1/2; (viii) −x+1/2, y+1/2, z−1/2; (ix) x−1/2, −y+1/2, −z−1/2; (x) −x, y−1/2, −z+1; (xi) −x+1/2, −y, z+1/2; (xii) −x+1/2, y−1/2, z+1/2; (xiii) x+1/2, −y+1/2, −z+1/2; (xiv) x+1/2, y, −z+1/2; (xv) −x+1, y−1/2, −z; (xvi) −x+1, −y+1, −z; (xvii) x+1/2, −y+1/2, −z−1/2; (xviii) −x, y+1/2, −z+1; (xix) −x, y+1/2, −z; (xx) −x+1/2, −y+1, z+1/2; (xxi) x−1/2, y, −z+1/2; (xxii) −x+1, y+1/2, −z; (xxiii) x, −y+3/2, z.

Table S4. Fractional atomic coordinates and isotropic or equivalent isotropic displacement parameters (Å^2) for CeO_2.

	x	*y*	*z*	B_{iso}*/B_{eq}
Ce1	0	0	0	0.1
O1	0.25	0.25	0.25	0.1

Table S5. Geometric parameters (Å, °) for CeO_2.

Ce1—O1^{i}	2.3431 (1)	O1—Ce1^{ix}	2.3431 (1)
Ce1—O1^{ii}	2.3431 (1)	O1—Ce1^{x}	2.3431 (1)
Ce1—O1^{iii}	2.3431 (1)	O1—Ce1	2.3431 (1)
Ce1—O1^{iv}	2.3431 (1)	O1—O1^{xi}	2.7056 (1)
Ce1—O1^{v}	2.3431 (1)	O1—O1^{ii}	2.7056 (1)
Ce1—O1^{vi}	2.3431 (1)	O1—O1^{vi}	2.7056 (1)
Ce1—O1^{vii}	2.3431 (1)	O1—O1^{v}	2.7056 (1)
Ce1—O1	2.3431 (1)	O1—O1^{xii}	2.7056 (1)
O1—Ce1^{viii}	2.3431 (1)	O1—O1^{xiii}	2.7056 (1)
O1^{ii}—Ce1—O1^{i}	70.529	O1^{xi}—O1—Ce1^{viii}	125.264
O1^{iii}—Ce1—O1^{ii}	180	O1^{ii}—O1—O1^{xi}	90
O1^{iii}—Ce1—O1^{i}	109.471	O1^{ii}—O1—Ce1	54.736
O1^{iv}—Ce1—O1^{iii}	109.471	O1^{ii}—O1—Ce1^{x}	125.264
O1^{iv}—Ce1—O1^{ii}	70.529	O1^{ii}—O1—Ce1^{ix}	54.736
O1^{iv}—Ce1—O1^{i}	109.471	O1^{ii}—O1—Ce1^{viii}	125.264
O1^{v}—Ce1—O1^{iv}	70.529	O1^{vi}—O1—O1^{ii}	90
O1^{v}—Ce1—O1^{iii}	70.529	O1^{vi}—O1—O1^{xi}	90
O1^{v}—Ce1—O1^{ii}	109.471	O1^{vi}—O1—Ce1	54.736
O1^{v}—Ce1—O1^{i}	180	O1^{vi}—O1—Ce1^{x}	54.736
O1^{vi}—Ce1—O1^{v}	109.471	O1^{vi}—O1—Ce1^{ix}	125.264

$O1^{vi}$—Ce1—$O1^{iv}$	180	$O1^{vi}$—O1—$Ce1^{viii}$	125.264
$O1^{vi}$—Ce1—$O1^{iii}$	70.529	$O1^{v}$—O1—$O1^{vi}$	90
$O1^{vi}$—Ce1—$O1^{ii}$	109.471	$O1^{v}$—O1—$O1^{ii}$	90
$O1^{vi}$—Ce1—$O1^{i}$	70.529	$O1^{v}$—O1—$O1^{xi}$	180
$O1^{vii}$—Ce1—$O1^{vi}$	109.471	$O1^{v}$—O1—Ce1	54.736
$O1^{vii}$—Ce1—$O1^{v}$	109.471	$O1^{v}$—O1—$Ce1^{x}$	125.264
$O1^{vii}$—Ce1—$O1^{iv}$	70.529	$O1^{v}$—O1—$Ce1^{ix}$	125.264
$O1^{vii}$—Ce1—$O1^{iii}$	70.529	$O1^{v}$—O1—$Ce1^{viii}$	54.736
$O1^{vii}$—Ce1—$O1^{ii}$	109.471	$O1^{xii}$—O1—$O1^{v}$	90
$O1^{vii}$—Ce1—$O1^{i}$	70.529	$O1^{xii}$—O1—$O1^{vi}$	90
O1—Ce1—$O1^{vii}$	180	$O1^{xii}$—O1—$O1^{ii}$	180
O1—Ce1—$O1^{vi}$	70.529	$O1^{xii}$—O1—$O1^{xi}$	90
O1—Ce1—$O1^{v}$	70.529	$O1^{xii}$—O1—Ce1	125.264
O1—Ce1—$O1^{iv}$	109.471	$O1^{xii}$—O1—$Ce1^{x}$	54.736
O1—Ce1—$O1^{iii}$	109.471	$O1^{xii}$—O1—$Ce1^{ix}$	125.264
O1—Ce1—$O1^{ii}$	70.529	$O1^{xii}$—O1—$Ce1^{viii}$	54.736
O1—Ce1—$O1^{i}$	109.471	$O1^{xiii}$—O1—$O1^{xii}$	90
$Ce1^{ix}$—O1—$Ce1^{viii}$	109.471	$O1^{xiii}$—O1—$O1^{v}$	90
$Ce1^{x}$—O1—$Ce1^{ix}$	109.471	$O1^{xiii}$—O1—$O1^{vi}$	180
$Ce1^{x}$—O1—$Ce1^{viii}$	109.471	$O1^{xiii}$—O1—$O1^{ii}$	90
Ce1—O1—$Ce1^{x}$	109.471	$O1^{xiii}$—O1—$O1^{xi}$	90
Ce1—O1—$Ce1^{ix}$	109.471	$O1^{xiii}$—O1—Ce1	125.264
Ce1—O1—$Ce1^{viii}$	109.471	$O1^{xiii}$—O1—$Ce1^{x}$	125.264
$O1^{xi}$—O1—Ce1	125.264	$O1^{xiii}$—O1—$Ce1^{ix}$	54.736
$O1^{xi}$—O1—$Ce1^{x}$	54.736	$O1^{xiii}$—O1—$Ce1^{viii}$	54.736

$O1^{xi}$—O1—$Ce1^{ix}$	54.736

Symmetry codes: (i) −x, z, −y; (ii) −x, z, y; (iii) z, −x, −y; (iv) −x, −y, z; (v) z, −x, y; (vi) z, y, −x; (vii) −x, −z, −y; (viii) x+1/2, y, z+1/2; (ix) x, y+1/2, z+1/2; (x) x+1/2, y+1/2, z; (xi) z, −x+1, y; (xii) −x+1, z, y; (xiii) z, y, −x+1.

S6.2 Agreement Between Simulation and Empirical Structure Determinations

Synchrotron XRD data for the CCTM powder is displayed in **Figure S3a**, with the red ticks at the bottom denoting the positions of reflections simulated from the SCAN+*U*-computed CCTM2112 structure using the GSAS-II code.[20] The ADDSYM tool[21,22] was run on the unit cell derived from the SCAN+*U* calculation, which added an inversion center and assigned the higher symmetry space group, *Pnma* (space group 62), to the structural model. Converting from supercell to unit cell yielded lattice parameters of a = 5.567 Å, b = 7.640 Å, and c = 5.377 Å, with bond angles rounded to α = β = γ = 90°. The indexed structure was further refined using the GSAS-II program,[20] and a comparison of the diffraction pattern simulated from the refined CCTM2112 structure was overlaid with the experimental XRD in **Figure S3b**, firmly establishing agreement between the SCAN+*U* structural model and the structure of the as-synthesized CCTM2112 powder.

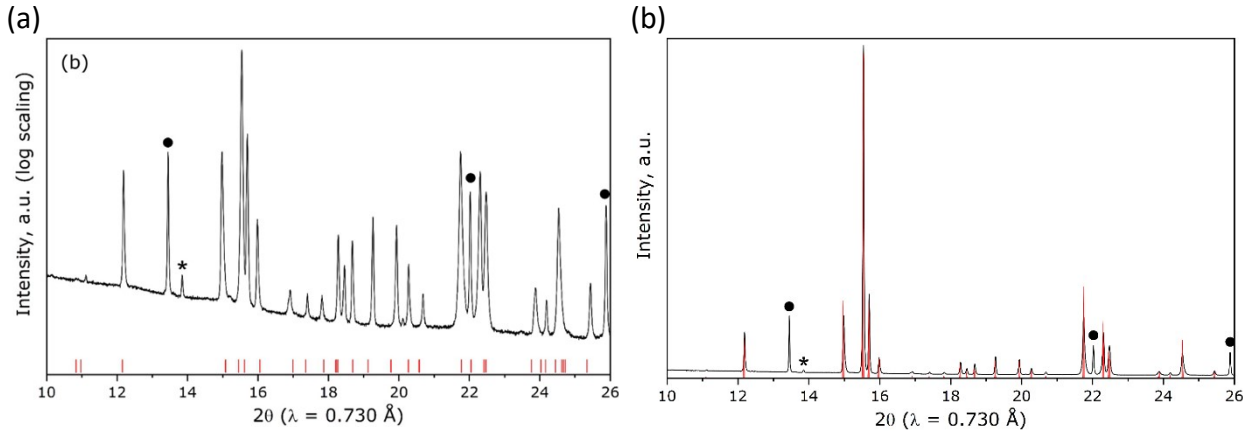

Figure S3. (a) Logarithmically scaled XRD data from the as-synthesized CCTM powder. Locations of reflections simulated from the SCAN+*U*-optimized structure are shown by red tick marks. Solid circles identify reflections from CeO_2. The asterisk denotes the location of a reflection corresponding to putty used to seal the capillary. The intensities are logarithmically scaled to highlight agreement between simulation and XRD even for low intensity diffraction peaks. (b) Linearly scaled XRD data from the as-synthesized CCTM powder with simulated diffraction pattern (with artificial instrumental broadening) from the computationally modeled CCTM unit cell is shown in the overlaid red diffraction pattern. The solid circles identify reflections from CeO_2. The asterisk denotes the location of a reflection corresponding to putty used to seal the capillary.

S7. Supporting Results

Table S6. Comparison of the probability (Pr) and percentage (probability expressed as %) of all unique NN V_O environments, where x_S and N_S are the mole fraction and number of species *S* in the NN V_O environment, respectively, in the random alloy and the optimized SQS for *Pnma* CCTM2112 (% in SQS). If the site occupancy follows the binomial distribution, the probability of the V_O having exactly k_S NNs of species *S* in N noninteracting sites is given by $\binom{N}{k_S} p_S^{k_S} (1-p_S)^{N-k_S}$. $\binom{N}{k_S} = \frac{N!}{k_S!(N-k_S)!}$ is the binomial coefficient and p_S is probability of choosing *S* based on the composition (p_{Ce} = 1/3 and p_{Mn} = 2/3). Pr(A) and Pr(B) are the probability of the NN A- and B-site combination, respectively, and Pr = Pr(A) × Pr(B). $Pr(A) = \binom{4}{4x_{Ce}} \left(\frac{1}{3}\right)^{4x_{Ce}} \left(\frac{2}{3}\right)^{4(1-x_{Ce})}$ and $Pr(B) = \binom{2}{2x_{Mn}} \left(\frac{2}{3}\right)^{2x_{Mn}} \left(\frac{1}{3}\right)^{2(1-x_{Mn})}$, where we used $k_{Ce} = 4x_{Ce}$ (because each V_O has N = 4 A-site NNs) and $k_{Mn} = 2x_{Mn}$ (because each V_O has N = 2 B-site NNs). The x_{Ce} = 1 and x_{Mn} = 0 NN environment does not appear in the SQS because its frequency in the random alloy is 0.30, i.e., < 1 out of 216 atoms. On the other hand, the x_{Ce} = 1 and x_{Mn} = 0.5 NN environment does not appear in the SQS because it was randomly selected instead of the x_{Ce} = 1 and x_{Mn} = 1 NN environment, which has the same probability in the random alloy.

x_{Ce}	x_{Mn}	N_{Ca}	N_{Ce}	Pr(A)	N_{Ti}	N_{Mn}	Pr(B)	Pr	%	% in SQS
0.00	1.00	4	0	0.20	0	2	0.44	0.09	8.8%	10.2%
0.00	0.50	4	0	0.20	1	1	0.44	0.09	8.8%	7.4%
0.00	0.00	4	0	0.20	2	0	0.11	0.02	2.2%	1.9%
0.25	1.00	3	1	0.40	0	2	0.44	0.18	17.6%	16.2%
0.25	0.50	3	1	0.40	1	1	0.44	0.18	17.6%	20.4%
0.25	0.00	3	1	0.40	2	0	0.11	0.04	4.4%	4.2%
0.50	1.00	2	2	0.30	0	2	0.44	0.13	13.2%	11.1%
0.50	0.50	2	2	0.30	1	1	0.44	0.13	13.2%	13.9%
0.50	0.00	2	2	0.30	2	0	0.11	0.03	3.3%	3.2%
0.75	1.00	1	3	0.10	0	2	0.44	0.04	4.4%	5.1%
0.75	0.50	1	3	0.10	1	1	0.44	0.04	4.4%	3.7%
0.75	0.00	1	3	0.10	2	0	0.11	0.01	1.1%	1.4%
1.00	1.00	0	4	0.01	0	2	0.44	0.01	0.5%	1.4%
1.00	0.50	0	4	0.01	1	1	0.44	0.01	0.5%	0.0%
1.00	0.00	0	4	0.01	2	0	0.11	0.00	0.1%	0.0%

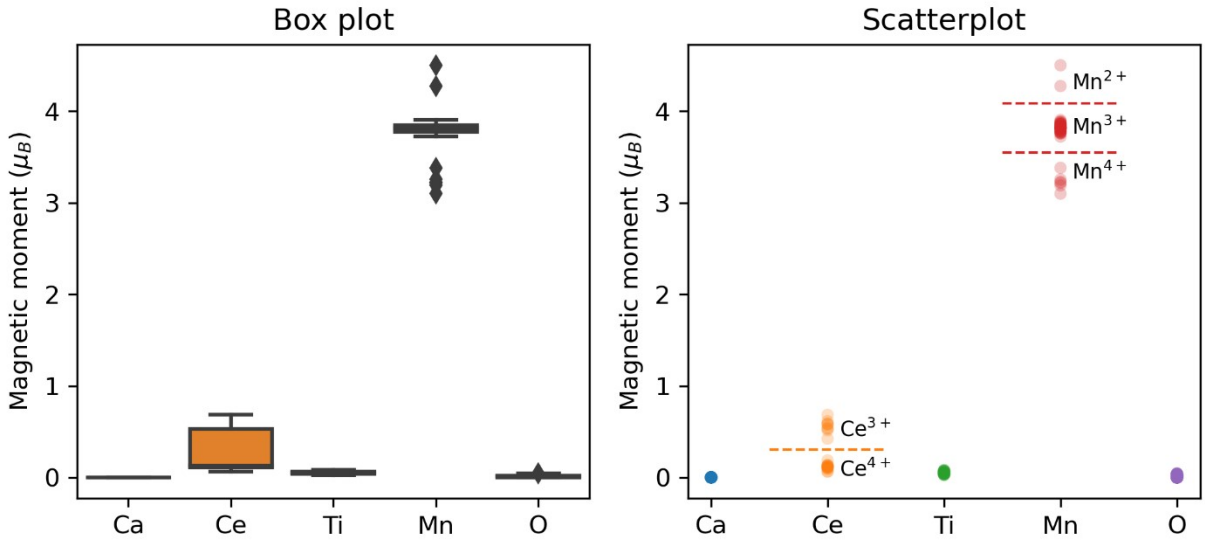

Figure S4. Magnetic moment distribution by species in pristine CCTM2112 from SCAN+*U* as a box plot (left panel) and a scatterplot (right panel). The box shows the quartiles of the dataset while the whiskers extend to show the rest of the distribution, except for points that are determined to be outliers, i.e., those outside 1.5× the inter-quartile range (diamonds). Dashed lines in the scatterplot are those that have the largest distance to the nearest data point of any cluster. Since Ce has two non-zero oxidation states (4+ and 3+), we plot one orange dashed line at the magnetic moment best separating Ce^{4+} and Ce^{3+}, i.e., 0.31 μ_B. Since, rounded to the nearest integer, Mn has an oxidation state of 3+ and two other stable non-zero oxidation states (4+ and 2+), we plot two red dashed lines at the magnetic moments best separating Mn^{4+} and Mn^{3+}, i.e., 3.55 μ_B, and Mn^{3+} and Mn^{2+}, i.e., 4.09 μ_B.

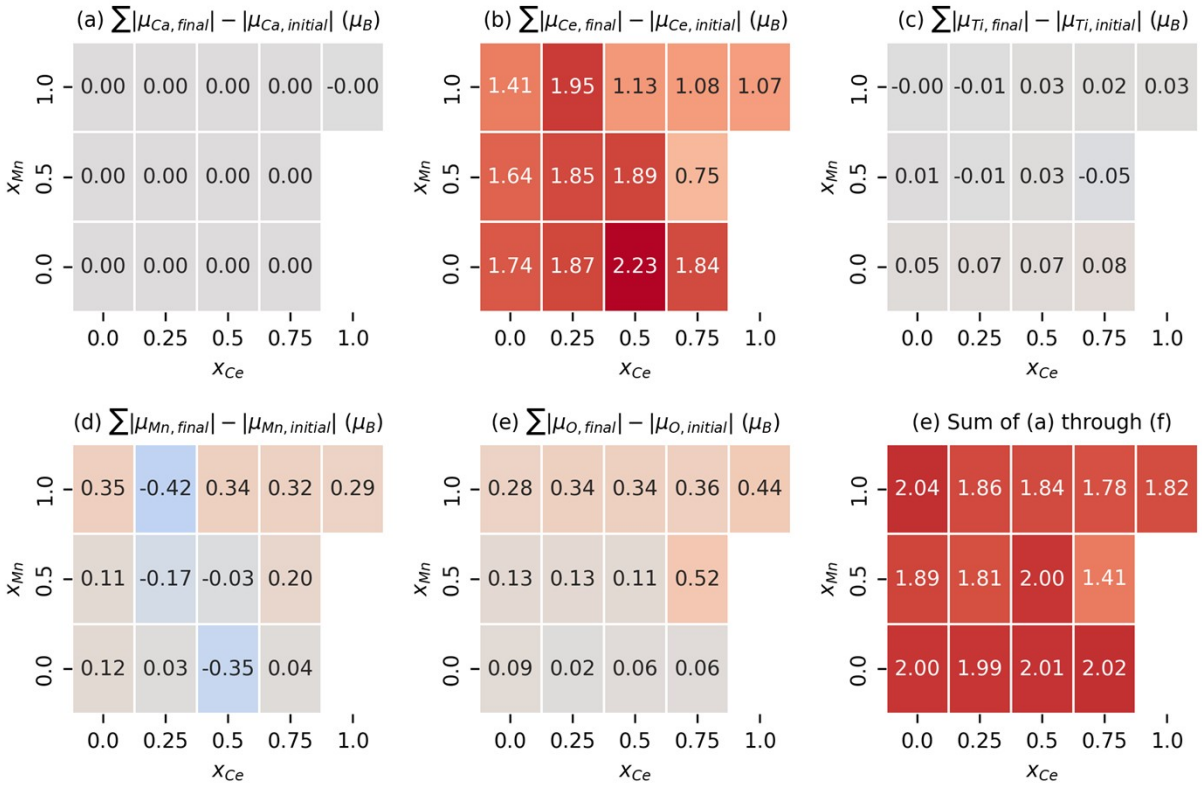

Figure S5. Dependence of V_O-induced magnetic moment changes in CCTM2112 for (a) Ca, (b) Ce, (c) Ti, (d) Mn, and (e) O on the V_O's NN environment, where the mole fractions, x, refer just to the NN environment, from SCAN+*U*. Panel (e) shows the sum of panels (a) through (f), with each entry being less than or approximately equal to two because neutral V_O formation involves a two-electron reduction of the lattice.

Table S7. Qualitative Ce and Mn oxidation state changes upon neutral V_O formation, designated by a slash, with red signifying reduction and blue oxidation. **Figure S4** shows how we assigned qualitative oxidation states to Ce and Mn (i.e., find lines best separating different cation clusters). Qualitative oxidation state changes that do not sum to two electrons (e^-) correspond to cases where the V_O induces delocalized electronic reorganization, which, e.g., can reduce the O sub-lattice.

Index	x_{Ce}	x_{Mn}	Frequency	Ce redox	Mn redox	Net redox
1	0.25	0.50	44	2 Ce4/3	1 Mn4/3, 1 Mn3/4	2 e^-
2	0.25	1.00	35	3 Ce4/3	1 Mn3/4	2 e^-
3	0.50	0.50	30	2 Ce4/3	None	2 e^-
4	0.50	1.00	24	3 Ce4/3, 1 Ce3/4	1 Mn4/3, 1 Mn2/3	2 e^-
5	0.00	1.00	22	2 Ce4/3	2 Mn4/3, 2 Mn3/4	2 e^-
6	0.00	0.50	16	3 Ce4/3	None	3 e^-
7	0.75	1.00	11	1 Ce4/3	None	1 e^-
8	0.25	0.00	9	3 Ce4/3	None	3 e^-
9	0.75	0.50	8	1 Ce4/3, 1 Ce3/4	2 Mn4/3, 1 Mn2/3, 1 Mn3/4	0 e^-
10	0.50	0.00	7	2 Ce4/3	1 Mn3/4	1 e^-
11	0.00	0.00	4	2 Ce4/3	None	2 e^-
12	0.75	0.00	3	2 Ce4/3	None	2 e^-
13	1.00	1.00	3	None	None	0 e-

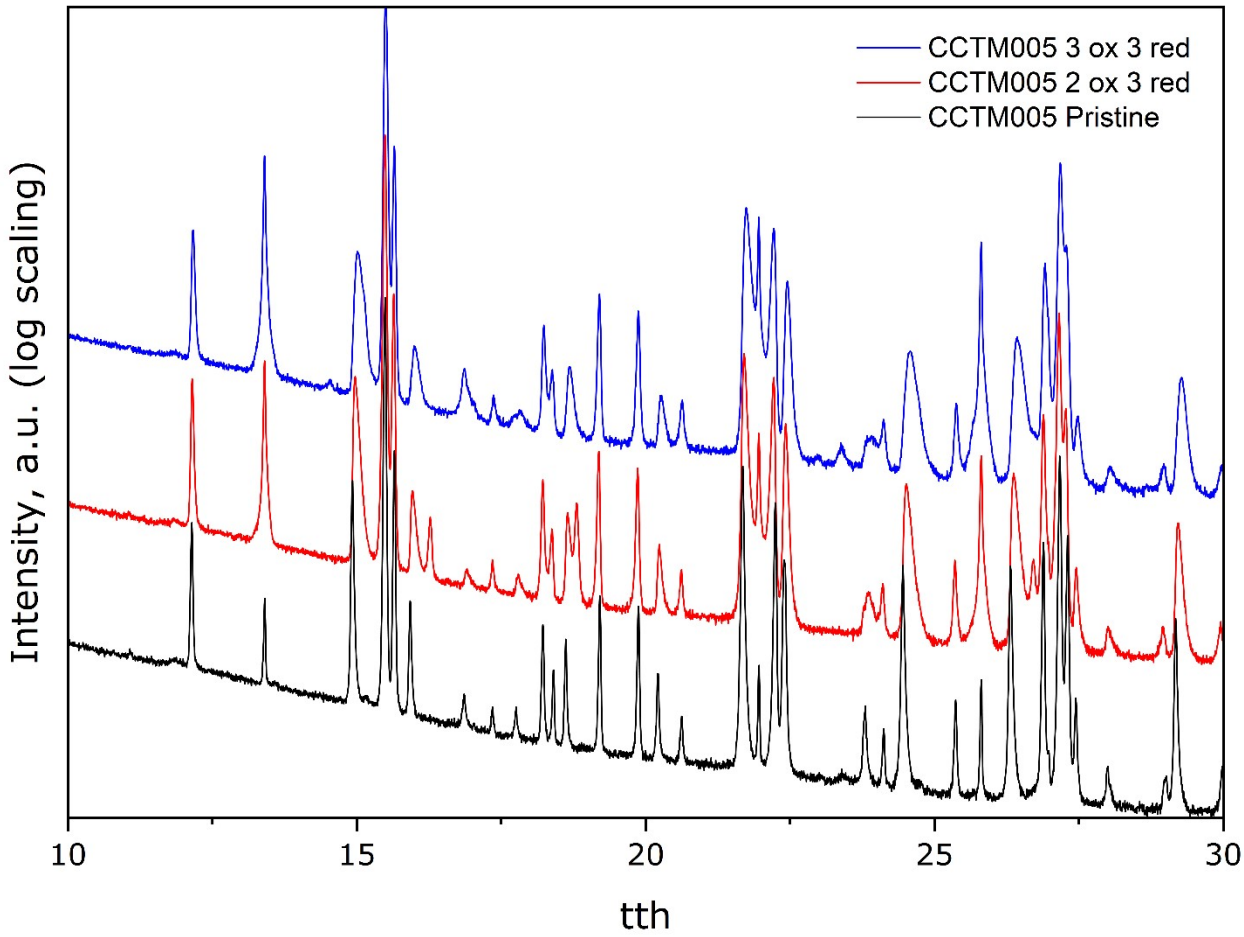

Figure S6. XRD of the as-synthesized (δ ≈ 0) CCTM material, as well as the material after a third reduction (i.e., three reductions and two re-oxidations) and third re-oxidation (i.e., three reductions and three re-oxidations). The horizontal axis is given in 2θ (tth) at a photon energy of 17 keV at Beamline 2-1 at the SSRL synchrotron at SLAC National Laboratory. Additional CeO_2 formation occurs during initial cycling. Additionally, Mn_3O_4 formation is also detected in the cycled material.

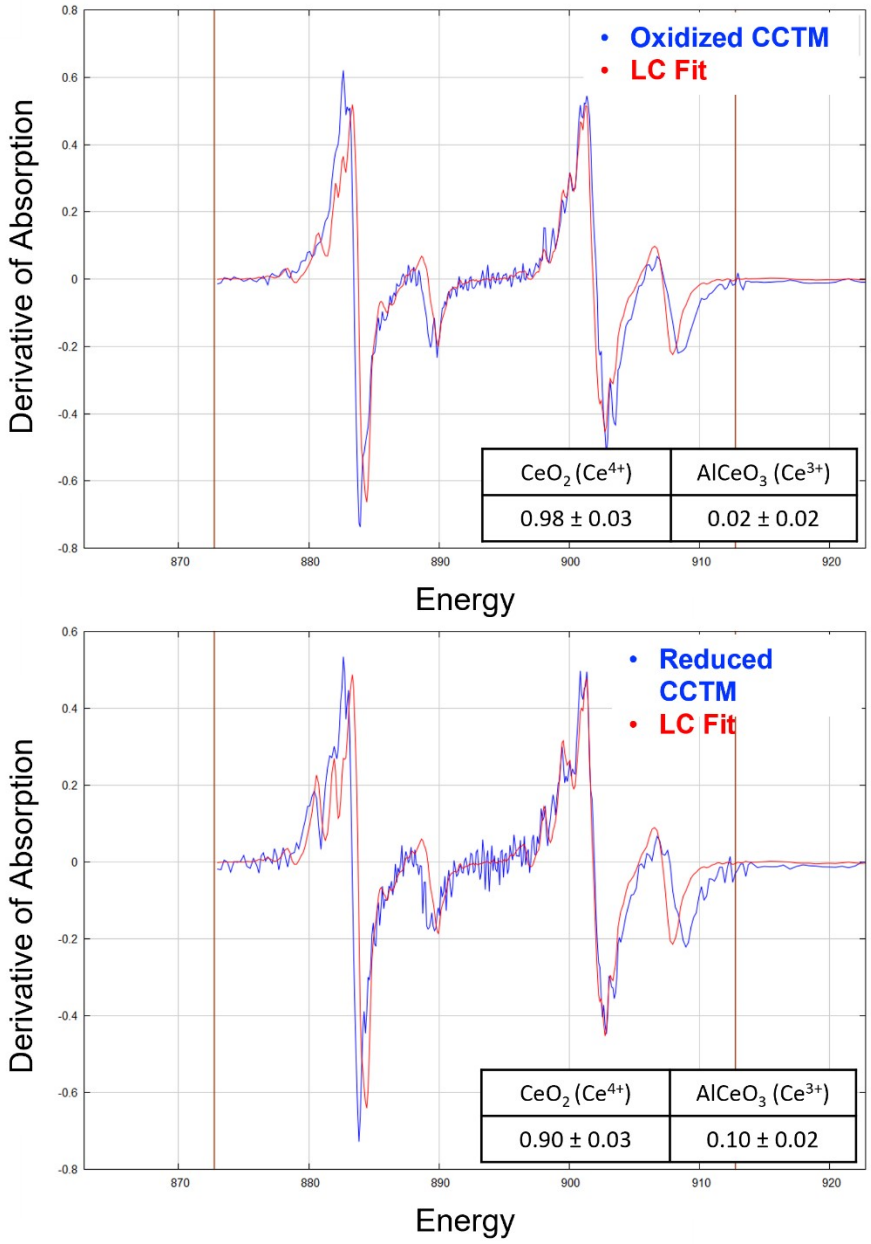

Figure S7. Derivative of the XAS spectra at the Ce 3d edge for oxidized CCTM (top) and reduced CCTM (bottom) overlaid with the fit resulting from a linear combination of the CeO_2 and $AlCeO_3$ standards (quantitative fit results provided in tables).

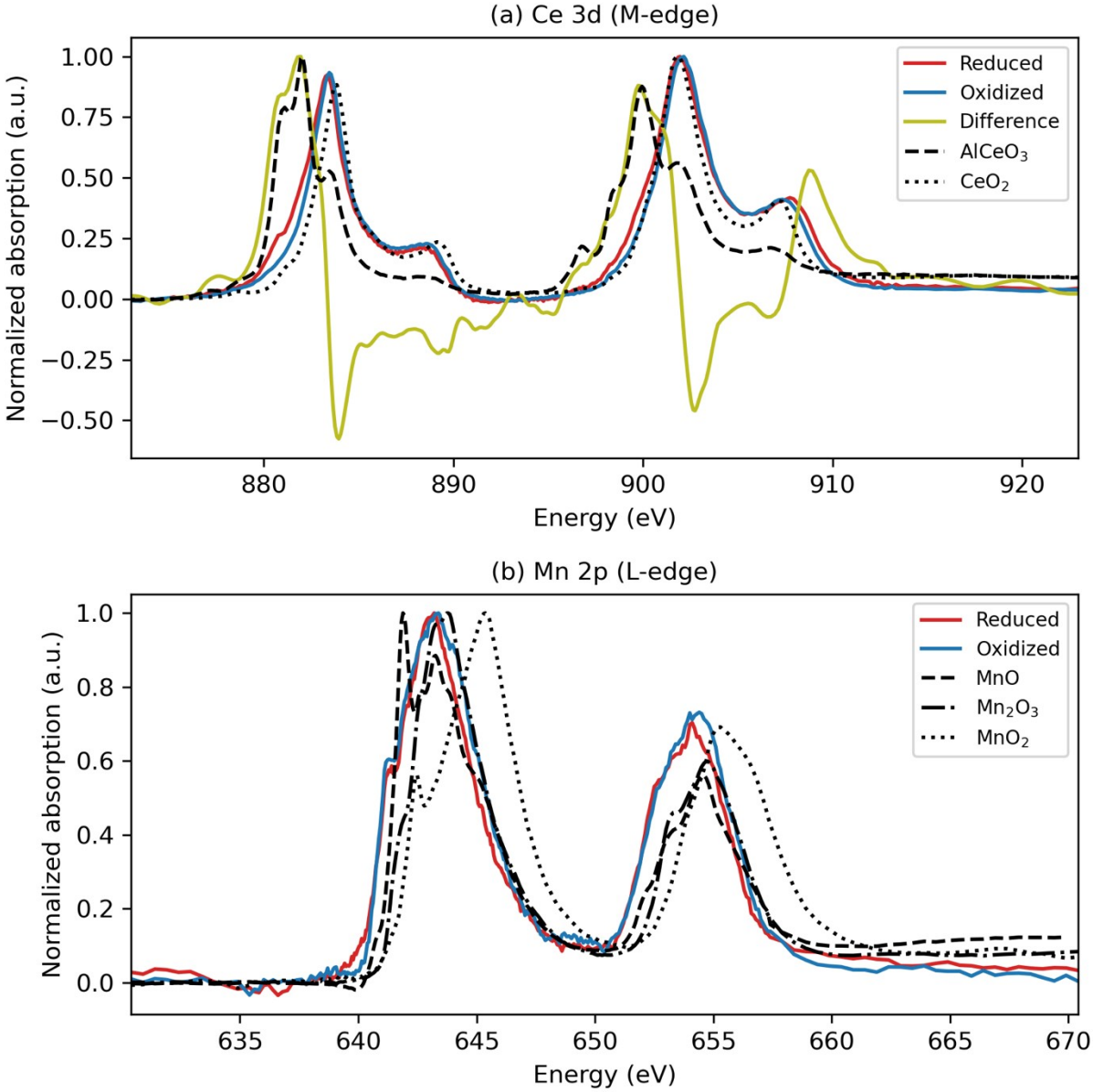

Figure S8. XAS spectra at the Ce $3d_{5/2}$ edge (a) for reduced CCTM2112, oxidized CCTM2112, the difference between reduced and oxidized CCTM2112 (Difference = Reduced – Oxidized), $AlCeO_3$ (Ce^{3+}) standard, and CeO_2 (Ce^{4+}) standard and Mn $2p_{3/2}$ spectra (b) for reduced CCTM2112, oxidized CCTM2112, MnO (Mn^{2+}) standard, Mn_2O_3 (Mn^{3+}) standard, and MnO_2 (Mn^{4+}) standard.

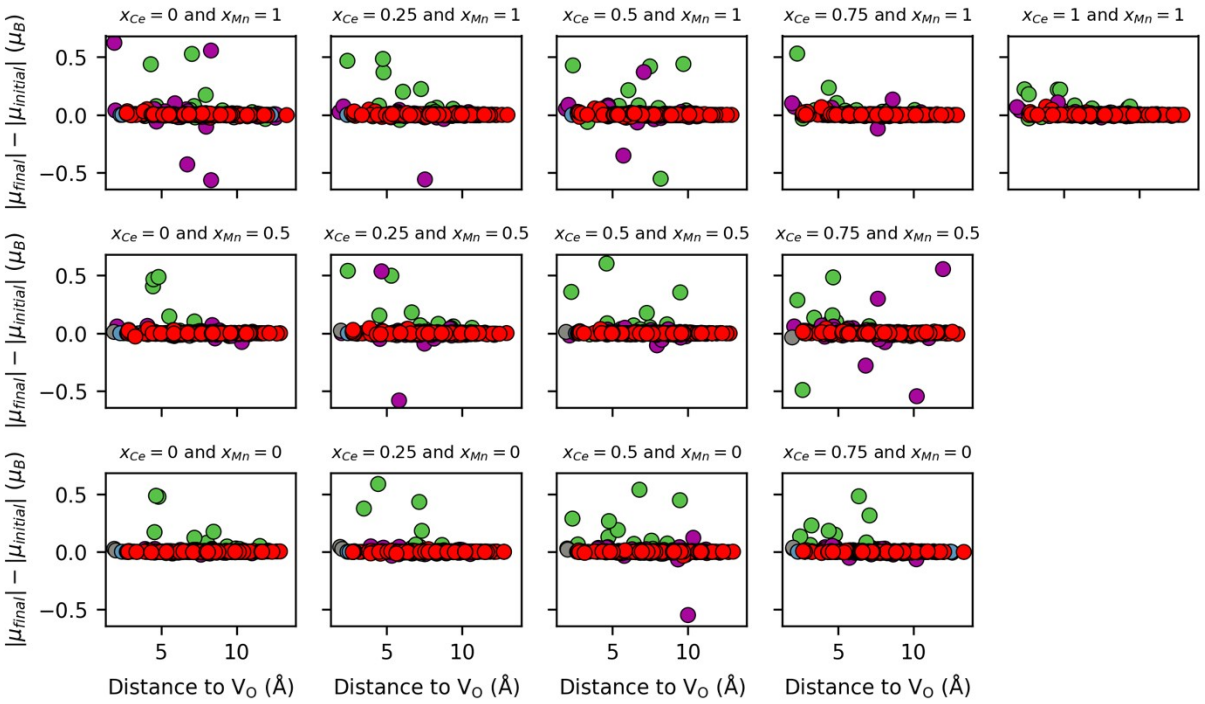

Figure S9. V_O-induced magnetic moment changes vs. distance for all NN VO environments considered in CCTM2112 from SCAN+*U*. Blue, green, gray, purple, and red data points correspond to Ca, Ce, Ti, Mn, and O, respectively.

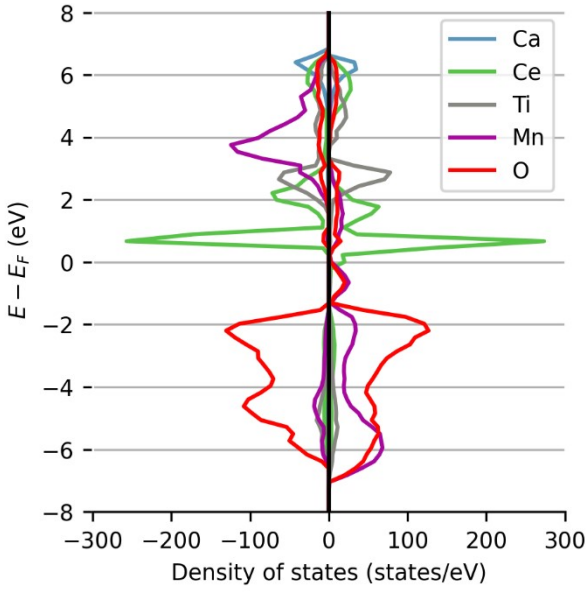

Figure S10. SCAN+*U* projected density of states of pristine CCTM2112 where E_F is the Fermi energy. Positive and negative densities of states correspond to opposite spin polarizations.

References

1. Kresse, G. & Hafner, J. Ab initio molecular dynamics for liquid metals. *Phys. Rev. B* **47,** 558–561 (1993).
2. Kresse, G. & Furthmüller, J. Efficient iterative schemes for ab initio total-energy calculations using a plane-wave basis set. *Phys. Rev. B* **54,** 11169–11186 (1996).
3. Sun, J., Ruzsinszky, A. & Perdew, J. P. Strongly Constrained and Appropriately Normed Semilocal Density Functional. *Phys. Rev. Lett.* **115,** 036402 (2015).
4. Anisimov, V. I., Zaanen, J. & Andersen, O. K. Band theory and Mott insulators: Hubbard *U* instead of Stoner I. *Phys. Rev. B* **44,** 943–954 (1991).
5. Liechtenstein, A. I., Anisimov, V. I. & Zaanen, J. Density-functional theory and strong interactions: Orbital ordering in Mott-Hubbard insulators. *Phys. Rev. B* **52,** R5467–R5470 (1995).
6. Anisimov, V. I., Aryasetiawan, F. & Lichtenstein, A. I. First-principles calculations of the electronic structure and spectra of strongly correlated systems: the LDA+*U* method. *J. Phys. Condens. Matter* **9,** 767–808 (1997).
7. Dudarev, S. L., Botton, G. A., Savrasov, S. Y., Humphreys, C. J. & Sutton, A. P. Electron-energy-loss spectra and the structural stability of nickel oxide: An LSDA+*U* study. *Phys. Rev. B* **57,** 1505–1509 (1998).
8. Sai Gautam, G. & Carter, E. A. Evaluating transition metal oxides within DFT-SCAN and SCAN+*U* frameworks for solar thermochemical applications. *Phys. Rev. Mater.* **2,** 095401 (2018).
9. Long, O. Y., Sai Gautam, G. & Carter, E. A. Evaluating optimal *U* for 3d transition-metal oxides within the SCAN+*U* framework. *Phys. Rev. Mater.* **4,** 045401 (2020).

10. Blöchl, P. E. Projector augmented-wave method. *Phys. Rev. B* **50,** 17953–17979 (1994).

11. Kresse, G. & Joubert, D. From ultrasoft pseudopotentials to the projector augmented-wave method. *Phys. Rev. B* **59,** 1758–1775 (1999).

12. Ong, S. P., Richards, W. D., Jain, A., Hautier, G., Kocher, M., Cholia, S., Gunter, D., Chevrier, V. L., Persson, K. A. & Ceder, G. Python Materials Genomics (pymatgen): A robust, open-source python library for materials analysis. *Comput. Mater. Sci.* **68,** 314–319 (2013).

13. Ong, S. P., Wang, L., Kang, B. & Ceder, G. Li−Fe−P−O_2 Phase Diagram from First Principles Calculations. *Chem. Mater.* **20,** 1798–1807 (2008).

14. Ong, S. P., Jain, A., Hautier, G., Kang, B. & Ceder, G. Thermal stabilities of delithiated olivine MPO_4 (M=Fe, Mn) cathodes investigated using first principles calculations. *Electrochem. Commun.* **12,** 427–430 (2010).

15. Wexler, R. B., Gautam, G. S., Stechel, E. B. & Carter, E. A. Factors Governing Oxygen Vacancy Formation in Oxide Perovskites. *J. Am. Chem. Soc.* **143,** 13212–13227 (2021).

16. Zunger, A., Wei, S.-H., Ferreira, L. G. & Bernard, J. E. Special quasirandom structures. *Phys. Rev. Lett.* **65,** 353–356 (1990).

17. Ångqvist, M., Muñoz, W. A., Rahm, J. M., Fransson, E., Durniak, C., Rozyczko, P., Rod, T. H. & Erhart, P. ICET – A Python Library for Constructing and Sampling Alloy Cluster Expansions. *Adv. Theory Simul.* **2,** 1900015 (2019).

18. Barcellos, D. R., Sanders, M. D., Tong, J., McDaniel, A. H. & O'Hayre, R. P. $BaCe_{0.25}Mn_{0.75}O_{3-\delta}$—a promising perovskite-type oxide for solar thermochemical hydrogen production. *Energy Environ. Sci.* **11,** 3256–3265 (2018).

19. Coelho, A. A. *TOPAS* and *TOPAS-Academic* : an optimization program integrating computer algebra and crystallographic objects written in C++. *J. Appl. Crystallogr.* **51,** 210–218 (2018).

20. Toby, B. H. & Von Dreele, R. B. *GSAS-II* : the genesis of a modern open-source all purpose crystallography software package. *J. Appl. Crystallogr.* **46,** 544–549 (2013).

21. Le Page, Y. Computer derivation of the symmetry elements implied in a structure description. *J. Appl. Crystallogr.* **20,** 264–269 (1987).

22. Le Page, Y. *MISSYM* 1.1 – a flexible new release. *J. Appl. Crystallogr.* **21,** 983–984 (1988).